THE TRADE-OFF BETWEEN UNIVERSALITY AND LABEL EFFICIENCY OF REPRESENTATIONS FROM CONTRASTIVE LEARNING

Anonymous authors
Paper under double-blind review

ABSTRACT

Pre-trained representations (a.k.a. foundation models) have recently become a prevalent learning paradigm, where one first pre-trains a representation using large-scale unlabeled data, and then learns simple classifiers on top of the representation using small labeled data from the downstream tasks. There are two key desiderata for the representation: *label efficiency* (the ability to learn an accurate classifier on top of the representation with a small amount of labeled data) and *universality* (usefulness across a wide range of downstream tasks). In this paper, we focus on one of the most popular instantiations of this paradigm: contrastive learning with linear probing, i.e., learning a linear predictor on the representation pre-trained by contrastive learning. We show that there exists a trade-off between the two desiderata so that one may not be able to achieve both simultaneously. Specifically, we provide analysis using a theoretical data model and show that, while more diverse pre-training data result in more diverse features for different tasks (improving universality), it puts less emphasis on task-specific features, giving rise to larger sample complexity for down-stream supervised tasks, and thus worse prediction performance. Guided by this analysis, we propose a contrastive regularization method to improve the trade-off. We validate our analysis and method empirically with systematic experiments using real-world datasets and foundation models.

1 INTRODUCTION

Representation pre-training is a recent successful approach that utilizes large-scale unlabeled data to address the challenges of scarcity of labeled data and distribution shift. Different from the traditional supervised learning approach using a large labeled dataset, representation learning first pre-trains a representation function using large-scale diverse unlabeled datasets by self-supervised learning (e.g., contrastive learning), and then learns predictors on the representation using small labeled datasets for downstream target tasks. The pre-trained model is commonly referred to as a *foundation model* (Bommasani et al., 2021), and has achieved good performance in many applications, e.g., BERT (Devlin et al., 2019), GPT-3 (Brown et al., 2020), CLIP (Radford et al., 2021), and Flamingo (Alayrac et al., 2022). To this end, we note that there are two properties that are key to their success: (1) *label efficiency*: with the pre-trained representation, only a small amount of labeled data is needed to learn accurate predictors for downstream target tasks; (2) *universality*: the pre-trained representation can be used across various downstream tasks.

In this work, we focus on *contrastive learning with linear probing* that learns a linear predictor on the representation pre-trained by contrastive learning, which is an exemplary pre-training approach (e.g., (Arora et al., 2019; Chen et al., 2020)). We highlight and study a fundamental trade-off between label efficiency and universality, though ideally one would like to have these two key properties simultaneously. Since pre-training on diverse data is widely used in practice, such a trade-off merits deeper investigation.

Theoretically, we provide an analysis of the features learned by contrastive learning, and how the learned features determine the downstream prediction performance and lead to the trade-off. We propose a *hidden representation data model*, which first generates a hidden representation contain-

ing various features, and then uses it to generate the label and the input. We first show that contrastive learning is essentially generalized nonlinear PCA that can learn *hidden features invariant to the transformations* used to generate positive pairs. We also point out that additional assumptions on the data and representations are needed to obtain non-vacuous guarantees for prediction performance. We thus consider a setting where the data are generated by linear functions of the hidden representation, and formally prove that the difference in the learned features leads to the trade-off. In particular, pre-training on more diverse data learns more diverse features and is thus useful for prediction on more tasks. But it also down-weights task-specific features, implying larger sample complexity for predictors and thus worse prediction performance on a specific task. This analysis inspires us to propose a general method – *contrastive regularization* – that adds a contrastive loss to the training of predictors to improve the accuracy on downstream tasks.

Empirically, we first perform controlled experiments to reveal the tradeoff. Specifically, we first pre-train on a specific dataset similar to that of the target task, and then incrementally add more datasets into pre-training. In the end, the pre-training data includes both datasets similar to the target task and those not so similar, which mimics the practical scenario that foundation models are pre-trained on diverse data to be widely applicable for various downstream tasks. Fig. 1 gives an example of this experiment: As we increase task diversity for contrastive learning, it increases the average accuracy on *all tasks* from 18.3% to 20.1%, while it harms the label efficiency of an individual task, on CIFAR-10 the accuracy drops from 88.5% to 76.4%. We also perform experiments on contrastive regularization, and demonstrate that it can *consistently improve* over the typical fine-tuning method across multiple datasets. In several cases, the improvement is significant: 1.3% test accuracy improvement for CLIP on ImageNet, 4.8% for MoCo v3 on GTSRB (see Table 1 and 2 for details). With these results, we believe that it is of importance to bring the community's attention to this trade-off and the forward path of foundation models.

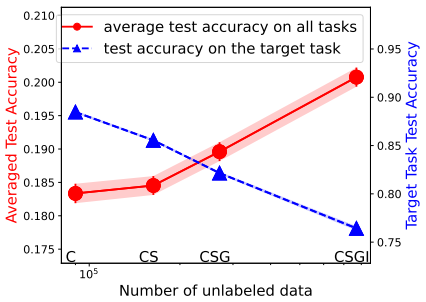

Figure 1: Illustration of the trade-off between universality and label efficiency. x-axis: from left to right, incrementally add CINIC-10 (C), SVHN (S), GTSRB (G), and ImageNet32 (I) for pre-training MoCo v2. For example, "CS" means CINIC-10+SVHN. The average test accuracy of prediction on all 4 datasets (red line) increases with more diverse pre-training data, while that on the target task CIFAR-10 (blue line) decreases. (The variance of blue line is too small to be seen.) Please refer to Section 3.1 for details.

Our main contributions are summarized as follows:

- We propose a hidden representation data model and prove that contrastive learning is essentially generalized nonlinear PCA, and can encode hidden features invariant to the transformations used in positive pairs (Section 2.1).
- We formally prove the trade-off in a simplified setting with linear data (Section 2.2).
- We empirically demonstrate the trade-off across different methods and datasets for contrastive learning with linear probing (Section 3.1 and 3.2).
- We propose a contrastive regularization method for training the predictor on a target task, which achieves consistent improvement in our experiments (Section 3.3).

Related Work on Representation Pre-training. This paradigm pre-trains a representation function on a large dataset and then uses it for prediction on various downstream tasks (Devlin et al., 2019; Kolesnikov et al., 2020; Brown et al., 2020; Newell & Deng, 2020). The representations are also called foundation models (Bommasani et al., 2021). There are mainly two kinds of approaches: (1) supervised approaches (e.g., (Kolesnikov et al., 2020)) that pre-train on large labeled datasets; (2) self-supervised approaches (e.g., (Newell & Deng, 2020)) that pre-train on large and diverse unlabeled datasets. Recent self-supervised pre-training can compete with or outperform supervised pre-training on the downstream prediction performance (Ericsson et al., 2021). Practical examples like BERT (Devlin et al., 2019), GPT-3 (Brown et al., 2020), CLIP (Radford et al., 2021), DALL·E (Ramesh et al., 2022), PaLM (Chowdhery et al., 2022) and Flamingo (Alayrac et al., 2022) have obtained effective representations universally useful for a wide range of downstream tasks.

A popular method is contrastive learning, i.e., to distinguish matching and non-matching pairs of augmented inputs (e.g., (van den Oord et al., 2018; Chen et al., 2020; He et al., 2020; Grill et al., 2020; Chen & He, 2021; Zbontar et al., 2021; Gao et al., 2021)). Some others solve "pretext tasks" like predicting masked parts of the inputs (e.g.,(Doersch et al., 2015; Devlin et al., 2019)).

Related Work on Analysis of Self-supervised Pre-training. There exist abundant studies analyzing self-supervised pre-training (Arora et al., 2019; Tsai et al., 2020; Yang et al., 2020; Wang & Isola, 2020; Garg & Liang, 2020; Zimmermann et al., 2021; Tosh et al., 2021; HaoChen et al., 2021; Wen & Li, 2021; Liu et al., 2021; Kotar et al., 2021; Van Gansbeke et al., 2021; Lee et al., 2021; Saunshi et al., 2022a; Shen et al., 2022; Kalibhat et al., 2022). They typically focus on pre-training or assume the same data distribution in pre-training and prediction. Since different distributions are the critical reason for the trade-off we focus on, we provide a new analysis. Some studies have connected contrastive learning to component analysis (Balestriero & LeCun, 2022; Tian, 2022; Ko et al., 2022). Our analysis focuses on the trade-off while also showing a connection to PCA based on our notion of invariant features and thus fundamentally different. Recently, Cole et al. have attempted to identify successful conditions for contrastive learning and point out the "diversity-difficulty trade-off", which is most relevant to our work. However, they only empirically show the trade-off, but provide no systematic study. Similarly, Bommasani et al. call for more research on specialization vs. diversity in pre-training data but providing no study. We aim to provide a better understanding of the trade-off between universality and label efficiency.

2 Theoretical Analysis

Our experiments in Section 3.1 demonstrate a trade-off between the universality and label efficiency of contrastively pre-trained representations when used for the prediction on a distribution different from the pre-training data distribution. See Figure 1 for an example. Intuitively, from the unlabeled data, pre-training can learn semantic features useful for prediction on even different data distributions. To analyze this, we need to formalize the notion of useful semantic features. So we introduce a *hidden representation data model* where a hidden representation (i.e., a set of semantic features) is sampled and then used for generating the data. Similar models have been used in some studies (HaoChen et al., 2021; Zimmermann et al., 2021), while we introduce the notions of spurious and invariant features and obtain a novel analysis for contrastive learning.

Using this theoretical model of data, Section 2.1 investigates what features are learned by contrastive learning. We show that *contrastive learning can be viewed as a generalization of Principal Components Analysis, and it encodes the invariant features not affected by the transformations but removes the others*. We also show that further assumptions on the data and the representations are needed necessary for any non-vacuous bounds for downstream prediction. So Section 2.2 considers a simplified setting with linear data. We show that when pre-trained on a mixture of unlabeled data from different tasks (i.e., diverse datasets), it encodes all invariant features from the different tasks and thus is useful for all tasks. On the other hand, it essentially emphasizes those that are shared among the tasks, but down-weights those that are specific to a single task. Compared to pre-training only on unlabeled data from the target task, this then leads to a larger sample complexity and thus worse generalization for prediction on the target task. Therefore, we show that the trade-off between universality and label efficiency occurs due to the fact that *when many useful features from diverse data are packed into the representation, those for a specific target task can be down-weighted and thus worsen the prediction performance on it*. Based on the insight, we propose a contrastive regularization method for using representations in downstream prediction tasks, which achieves consistent improvement over the typical fine-tuning method in our experiments in Section 3.3.

Contrastive Learning. Let $\mathcal{X} \subseteq \mathbb{R}^d$ denote the input space, $\mathcal{Y}$ the label space, and $\overline{\mathcal{Z}} \subseteq \mathbb{R}^k$ the output vector space of the learned representation function. Let Φ denote the hypothesis class of representation functions $\phi : \mathcal{X} \mapsto \overline{\mathcal{Z}}$, and $\mathcal{F}_\phi$ the hypothesis class of predictors on the representation ϕ. A task is simply a data distribution over $\mathcal{X} \times \mathcal{Y}$. In pre-training, using transformations on unlabeled data from the tasks, we have some pre-train distribution $\mathcal{D}_{pre}$ over positive pairs (x, x^+) and negative examples x^-, where x, x^+ are obtained by applying random transformations on the same input (e.g., cropping or color jitter for images), and x^- is an independent example. The contrastive loss is $\ell\left(\phi(x)^\top(\phi(x^+) - \phi(x^-))\right)$ where $\ell(\cdot)$ is a suitable loss function. Typically, it is $-\log \frac{\exp(\phi(x)^\top \phi(x^+))}{\exp(\phi(x)^\top \phi(x^+)) + \exp(\phi(x)^\top \phi(x^-))}$ with the logistic loss $\ell(t) = \log(1 + \exp(-t))$, while our

analysis also holds for more loss functions. A representation ϕ is learned by:

$$\min_{\phi \in \Phi} \mathbb{E}_{(x,x^+,x^-)\sim\mathcal{D}_{pre}} \left[\ell\left(\phi(x)^\top(\phi(x^+) - \phi(x^-))\right)\right]. \tag{1}$$

Then a predictor f is learned on top of ϕ using labeled data from a specific target task $\mathcal{D}$:

$$\min_{f \in \mathcal{F}_\phi} \mathbb{E}_{(x,y)\sim\mathcal{D}} \left[\ell_c(f(\phi(x)), y)\right] \tag{2}$$

where ℓ_c is a prediction loss (e.g. cross-entropy). Usually, f is a linear classifier (Linear Probing) with a bounded norm: $\mathcal{F}_\phi = \{f(z) = u^\top z : u \in \mathbb{R}^k, \|u\| \le B\}$, where $\|\cdot\|$ denotes the ℓ_2 norm.

Hidden Representation Data Model. We now consider the pre-train distribution $\mathcal{D}_{pre}$ over (x, x^+, x^-). To capture that pre-training can learn useful features, we assume a hidden representation for generating the data: first sample a hidden representation $z \in \mathcal{Z}$ from a distribution $\mathcal{D}_z$ over some hidden representation space $\mathcal{Z} \subseteq \mathbb{R}^d$, and then generate the input x and the label y from z. (The space $\mathcal{Z}$ models semantic features, and can be different from the learned representation space $\overline{\mathcal{Z}}$.) The dimensions of z are partitioned into two disjoint subsets of $[d] := \{1, \cdots, d\}$: *spurious features* U that are affected by the transformations, and *invariant features* R that are not. Specifically, let $\mathcal{D}_U, \mathcal{D}_R$ denote the distributions of z_U and z_R, respectively, and let $x = g(z)$ denote the generative function for x. Then the positive pairs (x, x^+) are generated as follows:

$$z = [z_R; z_U] \sim \mathcal{D}_z, z_U^+ \sim \mathcal{D}_U,\ z^+ = [z_R; z_U^+], \quad x = g(z), x^+ = g(z^+). \tag{3}$$

That is, x, x^+ are from the same z_R but two random copies of z_U that model the random transformations. Finally, x^- is an i.i.d. sample from the same distribution as x: $z^- \sim \mathcal{D}_z, x^- = g(z^-)$.

2.1 What Features are Learned by Contrastive Learning?

To analyze prediction performance, we first need to analyze what features are learned in pre-training.

Contrastive Learning is Generalized Nonlinear PCA. Recall that given data x from a distribution $\mathcal{D}$, Principal Components Analysis (PCA) (Pearson, 1901; Hotelling, 1933) aims to find a linear projection function ϕ on some subspace such that the variance of the projected data $\phi(x)$ is maximized, i.e., it is minimizing the following PCA objective:

$$-\mathbb{E}_{x\sim\mathcal{D}}[\|\phi(x) - \mathbb{E}_{x'\sim\mathcal{D}}[\phi(x')]\|^2] = -\mathbb{E}_{x\sim\mathcal{D}}[\|\phi(x) - \phi_0\|^2] \tag{4}$$

where $\phi_0 := \mathbb{E}[\phi(x')]$ is the mean of the projected data. Nonlinear PCA replaces linear representation functions ϕ with nonlinear ones. We next show that contrastive learning is a generalization of nonlinear PCA on the smoothed representation after smoothing out the transformations.

Theorem 2.1. *If $\ell(t) = -t$, then the contrastive loss is equivalent to the PCA objective on ϕ_{z_R}:*

$$\mathbb{E}\left[\ell\left(\phi(x)^\top[\phi(x^+) - \phi(x^-)]\right)\right] = -\mathbb{E}\left[\|\phi_{z_R} - \phi_0\|^2\right] \tag{5}$$

where $\phi_{z_R} := \mathbb{E}[\phi(x) \mid z_R] = \mathbb{E}[\phi(g(z)) \mid z_R]$. If additionally $\phi(x)$ is linear in x, then it is equivalent to the linear PCA objective $-\mathbb{E}\left[\|\phi(\bar{x}) - \phi_0\|^2\right]$ on data $\bar{x} := \mathbb{E}[x|z_R] = \mathbb{E}[g(z)|z_R]$.

So contrastive learning is essentially nonlinear PCA when $\ell(t) = -t$, and further specializes to linear PCA when the representation is linear. As PCA finds directions with large variances, the analogue is that contrastive learning encodes important invariant features but not the spurious ones.

Contrastive Learning Encodes Invariant Features and Removes Spurious Features. For a formal statement we need some weak assumptions on the data, the representations, and the loss:

- **(A1)** z_R can be recovered from x, i.e., the inputs $x = g(z)$ from different z_R's are disjoint.
- **(A2)** The representation functions are the *regular* functions with $\|\phi(x)\| = B_r$ $(\forall x)$ for some $B_r > 0$. Being regular means there are a finite L and a partition of $\mathcal{Z}$ into a finite number of subsets, such that in each subset all $\phi \circ g$ have Lipschitz constants bounded by L.
- **(A3)** The loss $\ell(t)$ is convex, decreasing, and lower-bounded.

The first condition means the invariant features z_R can be extracted from x (note that g need not be invertible). The regular condition on the representation is to exclude some pathological cases like

the Dirichlet function; essentially reasonable functions relevant for practice satisfy this condition, e.g., when g is Lipschitz and ϕ are neural networks with the ReLU activation. Also, note that the logistic loss typically used in practice satisfies the last condition.

We say a function $f(z)$ is independent of a subset of input dimensions z_S, if there exists a function f' such that $f(z) = f'(z_{-S})$ with probability 1, where z_{-S} denotes the set of all z_j's with $j \notin S$. We say the representation ϕ encodes a feature z_i, if $\phi \circ g : \mathcal{Z} \mapsto \overline{\mathcal{Z}}$ is not independent of z_i as long as the generative function $g(z)$ is not independent of z_i.

Theorem 2.2. *Under Assumptions **(A1)(A2)(A3)**, the optimal representation ϕ^* satisfies:*

(1) ϕ^* does not encode the spurious features z_U: $\phi^* \circ g(z)$ is independent of z_U.

(2) For any invariant feature $i \in R$, there exists $B_i > 0$ such that as long as the representations' norm $B_r \geq B_i$, then ϕ^* encodes z_i. Furthermore, if $\mathcal{Z}$ is finite, then B_i is monotonically decreasing in $\Pr[z_{R\setminus\{i\}} = z^-_{R\setminus\{i\}}, z_i \neq z_i^-]$, the probability that in z_R and z^-_R, the i-th feature varies while the others remain the same.

So contrastive learning aims to remove the spurious features and preserve the invariant features. Then the transformations should be chosen such that they will not affect the useful semantic features, but change those irrelevant to the label. Interestingly, the theorem further suggests that contrastive learning tends to favor the more "spread-out" invariant features z_i, as measured by $\Pr[z_{R\setminus\{i\}} = z^-_{R\setminus\{i\}}, z_i \neq z_i^-]$. As we increase the representation capacity B_r, B_r passes the threshold B_i for more features z_i, so ϕ^* first encodes the more spread-out invariant features and then the others.

This further suggests the following intuition for the trade-off. When pre-trained on diverse data that is a mixture from multiple tasks with different invariant features, the representation encodes all the invariant features and thus is useful for prediction on all the tasks. When pre-trained on only a specific task, features specific to this task are favored over those that only show up in other tasks, which leads to smaller sample complexity for learning the predictor and thus better prediction. However, to formalize this, some inductive bias assumptions about the data and the representation are necessary to get any non-vacuous guarantee for the prediction (see analysis in Appendix A.1). Therefore, Section 2.2 introduces additional assumptions and formalizes the trade-off.

2.2 Analyzing the Trade-Off: Linear Data

To analyze the prediction performance, we first need to model the relation between the pre-training data and the target task. We model the diverse pre-training data as a mixture of data from T different tasks $\mathcal{D}_t$'s, while the target task is one of the tasks (see empirical support in Section 3.2). All tasks share a public feature set S of size s, and each task $\mathcal{D}_t$ additionally owns a private disjoint feature set P_t of size $r - s$, i.e., $P_t \cap S = \emptyset$ and $P_{t_1} \cap P_{t_2} = \emptyset$ for $t_1 \neq t_2$ (Fig. 2). The invariant features for $\mathcal{D}_t$ are then $R_t = S \cup P_t$. All invariant features are $R = \cup_{t=1}^T R_t$, and spurious features are $U = [d] \setminus R$. In task $\mathcal{D}_t$, the (x, x^+) are generated as follows:

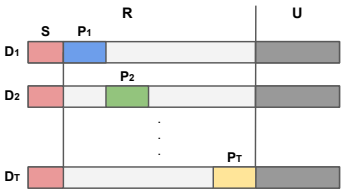

Figure 2: Illustration of the features in our data distributions.

$$z_{R_t} \sim \mathcal{N}(0, I),\ z_{R\setminus R_t} = 0,\ z_U \sim \mathcal{N}(0, I), z = [z_R; z_U], \quad x = g(z), \tag{6}$$

$$z_U^+ \sim \mathcal{N}(0, I), z^+ = [z_R; z_U^+], \quad x^+ = g(z^+), \tag{7}$$

and x^- is simply an i.i.d. copy from the same distribution as x. In practice, multiple independent negative examples are used, and thus we consider the following contrastive loss $\min_{\phi\in\Phi}\ \mathbb{E}_{(x,x^+)}\left[\ell\left(\phi(x)^\top(\phi(x^+) - \mathbb{E}_{x^-}\phi(x^-))\right)\right]$ for a convex and decreasing $\ell(t)$ to pre-train a representation ϕ. Then, when using ϕ for prediction in the target task $\mathcal{D}_t$, the predictor class should contain a predictor matching the ground-truth label:

$$\mathcal{F}_{\phi,t} = \{f(z) = u^\top z : u \in \mathbb{R}^k, \|u\| \leq B_{\phi,t}\} \tag{8}$$

where $B_{\phi,t}$ is the minimum value such that there exists $u_t \in \mathcal{F}_{\phi,t}$ with $y = u_t^\top \phi(x)$ on $\mathcal{D}_t$.

Now, given the necessity of inductive biases for non-vacuous guarantees (see Appendix A.1), and inspired by classic dictionary learning and recent analysis on such data (e.g., Olshausen & Field (1997); Wen & Li (2021); Shi et al. (2022)), we assume linear data and linear representations:

- x is linear in z: $x = g(z) = Mz$ where $M \in \mathbb{R}^{d\times d}$ is an orthonormal dictionary. Since linear probing has strong performance on pre-trained representations, we thus assume that the label in each task t is linear in its invariant features $y = (u_t^*)^\top z_{R_t}$ for some $u_t^* \in \mathbb{R}^r$.
- The representations are linear functions with weights of bounded spectral/Frobenius norms:
$$\Phi = \{\phi(x) = Wx : W\in\mathbb{R}^{k\times d}, \|W\|\leq 1, \|W\|_F\leq\sqrt{r}\}.$$
Here the norm bounds are chosen to be the minimum values to allow recovering the invariant features in the target task, i.e., there exists $\phi \in \Phi$ such that $\phi(x) = [z_{R_t}; \mathbf{0}]$.

We compare two representations: a specific one pre-trained on unlabeled data from the target task $\mathcal{D}_t$, and a universal one pre-trained on an even mixture of data from T tasks. (Appendix B provides analysis for more general cases like uneven mixtures.) This captures the situation that the pre-training data contains some data similar to the target task and also other less similar data. Let $v_{t,1} = \sum_{j\in S}(u_t^*)_j^2$ and $v_{t,2} = \sum_{j\in P_t}(u_t^*)_j^2$ be the weights on the shared and task-specific invariant features, respectively. Also, assume the prediction loss ℓ_c is L-Lipschitz.

Proposition 2.3. *The representation ϕ^* obtained on an even mixture of data from all the tasks $\{\mathcal{D}_t : 1 \leq t \leq T\}$ satisfies $\phi^*\circ g(z) = Q\left(\sum_{j\in S}\sqrt{\alpha}z_je_j + \sum_{j\in R\setminus S}\sqrt{\beta}z_je_j\right)$ for some $\alpha \in [0, 1]$, $\beta = \min\left(1, \frac{r-\alpha s}{T(r-s)}\right)$, where e_j's are the basis vectors and Q is any orthonormal matrix.*
The Empirical Risk Minimizer $\hat{u} \in \mathcal{F}_{\phi^*,t}$ on ϕ^* using m labeled data points from $\mathcal{D}_t$ has risk

$$\mathbb{E}_{(x,y)\sim\mathcal{D}_t}[\ell_c(\hat{u}^\top\phi^*(x), y)]$$
$$\leq 4L\sqrt{\frac{1}{m}\left(\frac{v_{t,1}}{\alpha} + \frac{v_{t,2}}{\beta}\right)}\left(\sqrt{s\alpha + (r-s)\beta} + O\left(\sqrt{\frac{r}{s\alpha + (r-s)\beta}}\right)\right) + 8\sqrt{\frac{2\ln(4/\delta)}{m}}.$$

Proposition 2.4. *The representation ϕ_t^* obtained on data from $\mathcal{D}_t$ satisfies $\phi_t^* \circ g(z) = Q\left(\sum_{j\in R_t} z_je_j\right)$ where e_j's are the basis vectors and Q is any orthonormal matrix.*
The Empirical Risk Minimizer $\hat{u} \in \mathcal{F}_{\phi_t^*,t}$ on ϕ_t^* using m labeled data points from $\mathcal{D}_t$ has risk

$$\mathbb{E}_{(x,y)\sim\mathcal{D}_t}[\ell_c(\hat{u}^\top\phi_t^*(x), y)] \leq 4L\sqrt{\frac{r}{m}}\|u_t^*\| + 8\sqrt{\frac{2\ln(4/\delta)}{m}}.$$

While on task $\mathcal{D}_i (i \neq t)$, any linear predictor on ϕ_t^* has error at least $\min_u \mathbb{E}_{\mathcal{D}_i}[\ell_c(u^\top z_S, y)]$.

Difference in Learned Features Leads to the Trade-off. The key of the analysis (in Appendix B) is about what features are learned in the representations. Pre-trained on all T tasks, ϕ^* is a rotation of the weighted features, where the shared features are weighted by $\sqrt{\alpha}$ and task-specific ones are weighted by $\sqrt{\beta}$. Pre-trained on one task $\mathcal{D}_t$, ϕ_t^* is a rotation of the task-specific features R_t. So compared to ϕ_t^*, ϕ^* encodes all invariant features but down-weights the task-specific features P_t.

The difference in the learned features then determines the prediction performance and results in a trade-off between universality and label efficiency: compared to ϕ_t^*, ϕ^* is useful for more tasks but has worse performance on the specific task $\mathcal{D}_t$. For illustration, suppose $r = 2s$, and the shared and task-specific features are equally important for the labels on the target task: $v_{t,1} = v_{t,2} = \|u_t^*\|^2/2$. We can show that ϕ^* has $\alpha = 1, \beta = \frac{1}{T}$ and the error is $O\left(L\sqrt{\frac{Tr}{m}}\|u_t^*\|\right)$, while the error using ϕ_t^* is $O\left(L\sqrt{\frac{r}{m}}\|u_t^*\|\right)$ (in Appendix B.3). Therefore, the error when using representations pre-trained on data from T tasks is $O(\sqrt{T})$ worse than that when just pre-training on data from the target task. On the other hand, the former can be used in all T tasks and the prediction error diminishes with the labeled data number m. While the latter only encodes R_t and the only useful features on the other tasks are z_S, then even with infinite labeled data the error can be large ($\geq \min_u \mathbb{E}[\ell_c(u^\top z_S, y)]$, the approximation error using only the common features z_S for prediction).

Improving the Trade-off via Contrastive Regularization. The above analysis provides some guidance on improving the trade-off, in particular, improving the target prediction accuracy when

given a pre-trained representation ϕ^*. It suggests that when ϕ^* is pre-trained on diverse data, one can update it by contrastive learning on some unlabeled data from the target task, which can get better features and better predictions. This is indeed the case for the illustrative example above. We can show that updating ϕ^* by contrastive learning on $\mathcal{D}_t$ can increase the weights β on the task-specific features z_{P_t}, and thus improve the generalization error (formal analysis in Appendix B.4).

In practice, typically one will have a labeled dataset $(x_i, y_i)_{i=1}^m$ from the target task, and will learn the classifier and also fine-tune the representation at the same time. We thus propose the following *contrastive regularization* for fine-tuning: generate contrastive pairs $\mathcal{R} = \{(\tilde{x}, \tilde{x}^+, \tilde{x}^-)\}$ by applying transformations on the input data x_i, and add the contrastive loss on these pairs as a regularization term to the classification loss,

$$\ell_c(f(\phi(\tilde{x})), y) + \frac{\lambda}{|\mathcal{R}|} \sum_{(\tilde{x}, \tilde{x}^+, \tilde{x}^-) \in \mathcal{R}} \ell\left(\phi(\tilde{x})^\top (\phi(\tilde{x}^+) - \phi(\tilde{x}^-))\right). \tag{9}$$

This method is simple and generally applicable to different models and algorithms. Similar ideas have been used in graph learning (Ma et al., 2021), domain generalization (Kim et al., 2021) and semi-supervised learning (Lee et al., 2022), while we use it in fine-tuning for learning predictors. Our experiments in Section 3.3 show that it can consistently improve the prediction performance compared to the typical fine-tuning approach.

3 Experiments

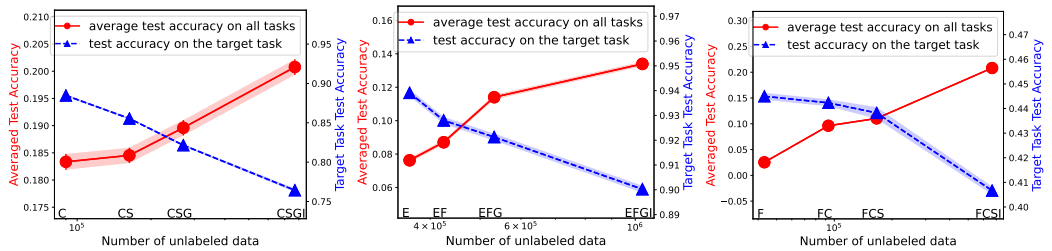

(a) CIFAR-10 (b) MNIST (c) Fer2013

Figure 3: Trade-off of universality and label efficiency for MoCo v2. Appendix C.5 shows similar results for more methods and datasets. x-axis: incrementally add datasets for pre-training MoCo v2. **(a)** Pre-training data: CINIC-10 (C), SVHN (S), GTSRB (G), and ImageNet32 (I). E.g., "CS" on the x-axis means CINIC-10+SVHN. Target task: CIFAR-10. Red line: average test accuracy of Linear Probing on all 4 datasets. Blue line: test accuracy on the target task. **(b)** EMNIST-Digits&Letters (E), Fashon-MNIST (F), GTSRB (G), ImageNet32 (I). Target: MNIST. **(c)** FaceScrub (F), CIFAR-10 (C), SVHN (S), ImageNet32 (I). Target: Fer2013.

We conduct experiments to answer the following questions. (**Q1**) Does the trade-off between universality and label efficiency exist when training on real datasets? (**Q2**) What factors leads to the trade-off? (**Q3**) How can we alleviate the trade-off, particularly in large foundation models?

Our experiments provide the following answers: (**A1**) The trade-off widely exists in different models and datasets, e.g. MoCo v2 on CIFAR-10 and so on (see Section 3.1). This justifies our study and aligns with our analysis. (**A2**) Different datasets own many private invariant features leading to the trade-off, e.g., FaceScrub and CIFAR-10 do not share many invariant features (see Section 3.2). It supports our analysis in Section 2.2. (**A3**) Our method proposed in Section 2.2, Finetune with Contrastive Regularization, can improve the trade-off consistently (see Section 3.3).

3.1 Verifying the Existence of the Trade-off

Evaluation & Methods. We pre-train a ResNet18 network (He et al., 2016) as a feature extractor under different contrastive learning methods. Then we fix the pre-trained feature extractor, and train a linear classifier (Linear Probing, LP) on the labeled data from the downstream task. We finally report the test accuracy on a specific target task and the average test accuracy on all

pre-training datasets (i.e., using them as the downstream tasks). We present full details and additional results in Appendix C.1, C.2 and C.5. Figure 3 shows the results for the method MoCo v2. The size and diversity of pre-training data is increased on the x-axis by incrementally adding unlabeled training data from: (a) CINIC-10, SVHN, GTSRB, ImageNet32 (using only a 500k subset); (b) EMNIST-Digits&Letters, Fashon-MNIST, GTSRB, ImageNet32; (c) FaceScrub, CIFAR-10, SVHN, ImageNet32.

Results. When the pre-training data becomes more diverse, the average test accuracy on all pre-training datasets increases (i.e., universality improves), while the test accuracy on the specific target task decreases (i.e., label efficiency drops). This shows a clear trade-off between universality and label efficiency. It supports our claim that diverse pre-training data allow learning diverse features for better universality, but can down-weight the features for a specific task resulting in worse prediction. Additional results in the appendix show similar trends (e.g., for methods NNCLR and SimSiam). This validates our analysis about the trade-off in Section 2.2.

3.2 Inspecting the Trade-off: Feature Similarity

For each set of pre-training data, we extract a set of features for the target task Fer2013 using the pre-trained representation function. Then we compute the similarities between different sets of features using linear Centered Kernel Alignment (CKA) (Kornblith et al., 2019), a widely used tool for high-dimensional feature comparison. This then reflects the similarity of the features learned from different pre-training data for the target task. Fig. 4 reports the results (rows/columns are pre-training data; numbers/colors show the similarity). The left figure shows the features from different pre-training datasets have low similarities. This is consistent with our setup in Section 2.2 that different tasks only share some features and each owns many private ones. The right figure shows a decreasing trend of similarity in each row. This indicates when gradually adding more diverse pre-training data, the obtained representation will encode more downstream task-irrelevant information and become less similar to that before adding more pre-training data. Additional results (e.g., for CIFAR-10, MNIST) with similar observations and some ablation studies are provided in Appendix C.3.

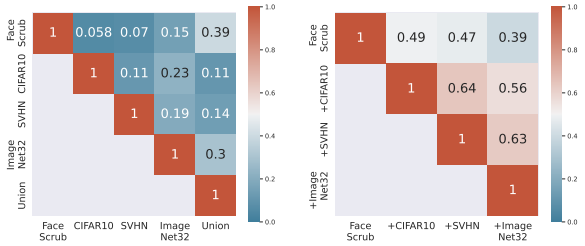

Figure 4: Linear CKA similarity among Fer2013 features from MoCo v2 pre-trained on different data. Left: each representation in the first four columns/rows is pre-trained on a single dataset. "Union" indicates the model pre-trained on the union among four disjoint datasets. Right: from left column to right, from top row to bottom, we incrementally add datasets for pre-training.

3.3 Improving the Trade-off: Finetune with Contrastive Regularization

Evaluation & Methods. Here we evaluate our contrastive regularization method proposed in Section 2.2. ResNet18 is pre-trained as in Section 3.1 by MoCo v2. Then we report the test accuracy on CIFAR-10 when the predictor is learned by: Linear Probing (LP), Finetune (FT), and Finetune with Contrastive Regularization (Ours). LP follows the training protocol in Section 3.1. FT and Ours learn a linear predictor and update the representation, and use the same data augmentation for fair comparison. FT follows the training in MAE (He et al., 2022), while Ours uses the contrastive loss from MoCo v2 and regularization coefficient $\lambda = 0.1$. More details and results are in Appendix C.4.

	Pre-training dataset			
Method	CINIC-10	+SVHN	+GTSRB	+ImageNet32
LP	88.41±0.01	85.18±0.01	82.07±0.01	75.64±0.03
FT	93.58±0.14	93.35±0.10	93.42±0.13	92.92±0.06
Ours	**94.51±0.02**	**94.26±0.01**	**94.32±0.13**	**93.66±0.12**

Table 1: Test accuracy on CIFAR-10 with different evaluation methods on MoCo v2. From left to right: incrementally add datasets for pre-training. More results are in Appendix C.4.

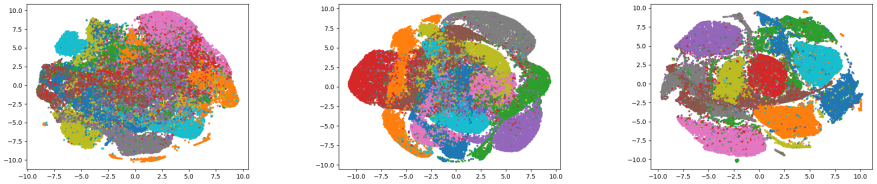

(a) Linear Probing (b) Finetune (c) Ours

Figure 5: The t-SNE visualization for CIFAR-10 training data normalized features from different evaluation methods, where model is pre-trained on (CSGI) defined in Fig. 3. FT and Ours are trained on 20% CIFAR-10 training dataset. Different colors correspond to different classes.

	CLIP			MoCo v3			SimCSE	
Method	ImageNet	SVHN	GTSRB	CIFAR-10	SVHN	GTSRB	IMDB	AGNews
LP	77.84±0.02	63.44±0.01	86.56±0.01	95.82±0.01	61.92±0.01	75.37±0.01	86.49±0.16	87.76±0.66
FT	83.65±0.01	78.22±0.18	90.74±0.06	96.17±0.12	65.36±0.33	76.45±0.29	92.31±0.26	93.57±0.23
Ours	**84.94±0.09**	**78.72±0.37**	**92.01±0.28**	**96.71±0.10**	**66.29±0.20**	**81.28±0.10**	**92.85±0.03**	**93.94±0.02**

Table 2: Test accuracy for different evaluation methods on different datasets using foundation models from CLIP, MoCo v3, and SimCSE. Data augmentation is not used for LP (Linear Probing). For FT (Finetune) and Ours (our method), 10 augmentations to each training images are used for CLIP, MoCo v3, and unique augmentation in each training step is used for SimCSE. More results are in Appendix C.4.1.

Results. Table 1 shows that our method can consistently outperform the other baselines. In particular, it outperforms the typical fine-tuning method by about 0.7%-1%, even when the latter also uses the same amount of data augmentation. This confirms the benefit of contrastive regularization. To further support our claim, Fig. 5 visualize the feature from different methods by t-SNE (Van der Maaten & Hinton, 2008). Contrastive regularization can highlight the task-specific features and provide a cleaner clustering, and thus improve the generalization, as discussed in Section 2.2.

Larger Foundation Models. We further evaluate our method on several popular real-world large representation models (foundation models). On some of these models, the user may be able to fine-tune the representation when learning predictors. On very large foundation models, the user typically extracts feature embeddings of their data from the models and then trains a small predictor, called adapter (Hu et al., 2021; Sung et al., 2022), on these embeddings. We evaluate CLIP (ViT-L as the representation backbone), MoCo v3 (ViT-B backbone), and SimCSE (Gao et al., 2021) (BERT backbone). They are trained on (image, text), (image, image), and (text, text) pairs, respectively, so cover a good spectrum of methods. For CLIP and MoCo v3, the backbone is fixed. LP uses a linear classifier, while FT and Ours insert a two-layer ReLU network as an adapter between the backbone and the linear classification layer. Ours uses the SimCLR contrastive loss on the output of the adapter. For SimCSE, all methods use linear classifiers. LP fixes the backbone, while FT and Ours train the classifier and fine-tune the backbone simultaneously. Ours uses the SimCSE contrastive loss on the backbone feature. We set regularization coefficient $\lambda = 1.0$.

Table 2 again shows our method can consistently improve the downstream prediction performance for all three models by about 0.4%-4.8%, and quite significantly in some cases (e.g., 1.3% for CLIP on ImageNet, 4.8% for MoCo v3 on GTSRB). This shows that the method is also useful for large foundation models, even when the foundation models cannot be fine-tuned and only the extracted embeddings can be adapted. Full details and more results are provided in Appendix C.4.1.

4 Discussion and Future Work

In this work, we have shown and analyzed the trade-off between label efficiency and universality of representations in contrastive learning. For future work, there are many open questions we will continue to study. (1) What features does the model learn from specific pre-training and diverse pre-training datasets beyond linear data? (2) Do the other self-supervised learning methods have similar trade-off? (3) Can we address the trade-off better to gain both properties at the same time?

REFERENCES

Jean-Baptiste Alayrac, Jeff Donahue, Pauline Luc, Antoine Miech, Iain Barr, Yana Hasson, Karel Lenc, Arthur Mensch, Katie Millican, Malcolm Reynolds, et al. Flamingo: a visual language model for few-shot learning. *arXiv preprint arXiv:2204.14198*, 2022.

Sanjeev Arora, Hrishikesh Khandeparkar, Mikhail Khodak, Orestis Plevrakis, and Nikunj Saunshi. A theoretical analysis of contrastive unsupervised representation learning. In *36th International Conference on Machine Learning, ICML 2019*, pp. 9904–9923. International Machine Learning Society (IMLS), 2019.

Randall Balestriero and Yann LeCun. Contrastive and non-contrastive self-supervised learning recover global and local spectral embedding methods. *arXiv preprint arXiv:2205.11508*, 2022.

Rishi Bommasani, Drew A. Hudson, Ehsan Adeli, Russ Altman, Simran Arora, Sydney von Arx, Michael S. Bernstein, Jeannette Bohg, Antoine Bosselut, Emma Brunskill, Erik Brynjolfsson, Shyamal Buch, Dallas Card, Rodrigo Castellon, Niladri S. Chatterji, Annie S. Chen, Kathleen Creel, Jared Quincy Davis, Dorottya Demszky, Chris Donahue, Moussa Doumbouya, Esin Durmus, Stefano Ermon, John Etchemendy, Kawin Ethayarajh, Li Fei-Fei, Chelsea Finn, Trevor Gale, Lauren Gillespie, Karan Goel, Noah D. Goodman, Shelby Grossman, Neel Guha, Tatsunori Hashimoto, Peter Henderson, John Hewitt, Daniel E. Ho, Jenny Hong, Kyle Hsu, Jing Huang, Thomas Icard, Saahil Jain, Dan Jurafsky, Pratyusha Kalluri, Siddharth Karamcheti, Geoff Keeling, Fereshte Khani, Omar Khattab, Pang Wei Koh, Mark S. Krass, Ranjay Krishna, Rohith Kuditipudi, and et al. On the opportunities and risks of foundation models. *CoRR*, abs/2108.07258, 2021. URL https://arxiv.org/abs/2108.07258.

Tom B. Brown, Benjamin Mann, Nick Ryder, Melanie Subbiah, Jared Kaplan, Prafulla Dhariwal, Arvind Neelakantan, Pranav Shyam, Girish Sastry, Amanda Askell, Sandhini Agarwal, Ariel Herbert-Voss, Gretchen Krueger, Tom Henighan, Rewon Child, Aditya Ramesh, Daniel M. Ziegler, Jeffrey Wu, Clemens Winter, Christopher Hesse, Mark Chen, Eric Sigler, Mateusz Litwin, Scott Gray, Benjamin Chess, Jack Clark, Christopher Berner, Sam McCandlish, Alec Radford, Ilya Sutskever, and Dario Amodei. Language models are few-shot learners. In *Advances in Neural Information Processing Systems 33: Annual Conference on Neural Information Processing Systems 2020, NeurIPS 2020, December 6-12, 2020, virtual*, 2020. URL https://proceedings.neurips.cc/paper/2020/hash/1457c0d6bfcb4967418bfb8ac142f64a-Abstract.html.

Ting Chen, Simon Kornblith, Mohammad Norouzi, and Geoffrey E. Hinton. A simple framework for contrastive learning of visual representations. In *Proceedings of the 37th International Conference on Machine Learning, ICML 2020, 13-18 July 2020, Virtual Event*, volume 119 of *Proceedings of Machine Learning Research*, pp. 1597–1607. PMLR, 2020. URL http://proceedings.mlr.press/v119/chen20j.html.

Xinlei Chen and Kaiming He. Exploring simple siamese representation learning. In *IEEE Conference on Computer Vision and Pattern Recognition, CVPR 2021, virtual, June 19-25, 2021*, pp. 15750–15758. Computer Vision Foundation / IEEE, 2021. URL https://openaccess.thecvf.com/content/CVPR2021/html/Chen_Exploring_Simple_Siamese_Representation_Learning_CVPR_2021_paper.html.

Aakanksha Chowdhery, Sharan Narang, Jacob Devlin, Maarten Bosma, Gaurav Mishra, Adam Roberts, Paul Barham, Hyung Won Chung, Charles Sutton, Sebastian Gehrmann, et al. Palm: Scaling language modeling with pathways. *arXiv preprint arXiv:2204.02311*, 2022.

Gregory Cohen, Saeed Afshar, Jonathan Tapson, and Andre Van Schaik. Emnist: Extending mnist to handwritten letters. In *2017 international joint conference on neural networks (IJCNN)*, pp. 2921–2926. IEEE, 2017.

Elijah Cole, Xuan Yang, Kimberly Wilber, Oisin Mac Aodha, and Serge Belongie. When does contrastive visual representation learning work? In *Proceedings of the IEEE/CVF Conference on Computer Vision and Pattern Recognition*, pp. 14755–14764, 2022.

Luke N Darlow, Elliot J Crowley, Antreas Antoniou, and Amos J Storkey. Cinic-10 is not imagenet or cifar-10. *arXiv preprint arXiv:1810.03505*, 2018.

Jia Deng, Wei Dong, Richard Socher, Li-Jia Li, Kai Li, and Li Fei-Fei. Imagenet: A large-scale hierarchical image database. In *2009 IEEE conference on computer vision and pattern recognition*, pp. 248–255. Ieee, 2009.

Jacob Devlin, Ming-Wei Chang, Kenton Lee, and Kristina Toutanova. BERT: pre-training of deep bidirectional transformers for language understanding. In *Proceedings of the 2019 Conference of the North American Chapter of the Association for Computational Linguistics: Human Language Technologies, NAACL-HLT 2019, Minneapolis, MN, USA, June 2-7, 2019, Volume 1 (Long and Short Papers)*, pp. 4171–4186. Association for Computational Linguistics, 2019. doi: 10.18653/v1/n19-1423. URL https://doi.org/10.18653/v1/n19-1423.

Carl Doersch, Abhinav Gupta, and Alexei A. Efros. Unsupervised visual representation learning by context prediction. In *2015 IEEE International Conference on Computer Vision, ICCV 2015, Santiago, Chile, December 7-13, 2015*, pp. 1422–1430. IEEE Computer Society, 2015. doi: 10.1109/ICCV.2015.167. URL https://doi.org/10.1109/ICCV.2015.167.

Debidatta Dwibedi, Yusuf Aytar, Jonathan Tompson, Pierre Sermanet, and Andrew Zisserman. With a little help from my friends: Nearest-neighbor contrastive learning of visual representations. In *Proceedings of the IEEE/CVF International Conference on Computer Vision*, pp. 9588–9597, 2021.

Linus Ericsson, Henry Gouk, and Timothy M. Hospedales. How well do self-supervised models transfer? In *IEEE Conference on Computer Vision and Pattern Recognition, CVPR 2021, virtual, June 19-25, 2021*, pp. 5414–5423. Computer Vision Foundation / IEEE, 2021. URL https://openaccess.thecvf.com/content/CVPR2021/html/Ericsson_How_Well_Do_Self-Supervised_Models_Transfer_CVPR_2021_paper.html.

Tianyu Gao, Xingcheng Yao, and Danqi Chen. Simcse: Simple contrastive learning of sentence embeddings. In *Proceedings of the 2021 Conference on Empirical Methods in Natural Language Processing*, pp. 6894–6910, 2021.

Siddhant Garg and Yingyu Liang. Functional regularization for representation learning: A unified theoretical perspective. *Advances in Neural Information Processing Systems*, 33:17187–17199, 2020.

Ian J Goodfellow, Dumitru Erhan, Pierre Luc Carrier, Aaron Courville, Mehdi Mirza, Ben Hamner, Will Cukierski, Yichuan Tang, David Thaler, Dong-Hyun Lee, et al. Challenges in representation learning: A report on three machine learning contests. In *International conference on neural information processing*, pp. 117–124. Springer, 2013.

Jean-Bastien Grill, Florian Strub, Florent Altché, Corentin Tallec, Pierre H. Richemond, Elena Buchatskaya, Carl Doersch, Bernardo Ávila Pires, Zhaohan Guo, Mohammad Gheshlaghi Azar, Bilal Piot, Koray Kavukcuoglu, Rémi Munos, and Michal Valko. Bootstrap your own latent - A new approach to self-supervised learning. In *Advances in Neural Information Processing Systems 33: Annual Conference on Neural Information Processing Systems 2020, NeurIPS 2020, December 6-12, 2020, virtual*, 2020. URL https://proceedings.neurips.cc/paper/2020/hash/f3ada80d5c4ee70142b17b8192b2958e-Abstract.html.

Jeff Z HaoChen, Colin Wei, Adrien Gaidon, and Tengyu Ma. Provable guarantees for self-supervised deep learning with spectral contrastive loss. *Advances in Neural Information Processing Systems*, 34, 2021.

Kaiming He, Xiangyu Zhang, Shaoqing Ren, and Jian Sun. Deep residual learning for image recognition. In *Proceedings of the IEEE conference on computer vision and pattern recognition*, pp. 770–778, 2016.

Kaiming He, Haoqi Fan, Yuxin Wu, Saining Xie, and Ross B. Girshick. Momentum contrast for unsupervised visual representation learning. In *2020 IEEE/CVF Conference on Computer Vision and Pattern Recognition, CVPR 2020, Seattle, WA, USA, June 13-19, 2020*, pp. 9726–9735. Computer Vision Foundation / IEEE, 2020. doi: 10.1109/CVPR42600.2020.00975. URL https://doi.org/10.1109/CVPR42600.2020.00975.

Kaiming He, Xinlei Chen, Saining Xie, Yanghao Li, Piotr Dollár, and Ross Girshick. Masked autoencoders are scalable vision learners. In *Proceedings of the IEEE/CVF Conference on Computer Vision and Pattern Recognition*, pp. 16000–16009, 2022.

Harold Hotelling. Analysis of a complex of statistical variables into principal components. *Journal of educational psychology*, 24(6):417, 1933.

Edward J Hu, Phillip Wallis, Zeyuan Allen-Zhu, Yuanzhi Li, Shean Wang, Lu Wang, Weizhu Chen, et al. Lora: Low-rank adaptation of large language models. In *International Conference on Learning Representations*, 2021.

Neha Mukund Kalibhat, Kanika Narang, Hamed Firooz, Maziar Sanjabi, and Soheil Feizi. Towards better understanding of self-supervised representations. In *ICML 2022: Workshop on Spurious Correlations, Invariance and Stability*, 2022.

Daehee Kim, Youngjun Yoo, Seunghyun Park, Jinkyu Kim, and Jaekoo Lee. Selfreg: Self-supervised contrastive regularization for domain generalization. In *Proceedings of the IEEE/CVF International Conference on Computer Vision*, pp. 9619–9628, 2021.

Ching-Yun Ko, Jeet Mohapatra, Sijia Liu, Pin-Yu Chen, Luca Daniel, and Lily Weng. Revisiting contrastive learning through the lens of neighborhood component analysis: an integrated framework. In *International Conference on Machine Learning*, pp. 11387–11412. PMLR, 2022.

Alexander Kolesnikov, Lucas Beyer, Xiaohua Zhai, Joan Puigcerver, Jessica Yung, Sylvain Gelly, and Neil Houlsby. Big transfer (bit): General visual representation learning. In *Computer Vision - ECCV 2020 - 16th European Conference, Glasgow, UK, August 23-28, 2020, Proceedings, Part V*, volume 12350 of *Lecture Notes in Computer Science*, pp. 491–507. Springer, 2020. doi: 10.1007/978-3-030-58558-7_29. URL https://doi.org/10.1007/978-3-030-58558-7_29.

Simon Kornblith, Mohammad Norouzi, Honglak Lee, and Geoffrey Hinton. Similarity of neural network representations revisited. In *International Conference on Machine Learning*, pp. 3519–3529. PMLR, 2019.

Klemen Kotar, Gabriel Ilharco, Ludwig Schmidt, Kiana Ehsani, and Roozbeh Mottaghi. Contrasting contrastive self-supervised representation learning pipelines. In *2021 IEEE/CVF International Conference on Computer Vision, ICCV 2021, Montreal, QC, Canada, October 10-17, 2021*, pp. 9929–9939. IEEE, 2021. doi: 10.1109/ICCV48922.2021.00980. URL https://doi.org/10.1109/ICCV48922.2021.00980.

Alex Krizhevsky, Geoffrey Hinton, et al. Learning multiple layers of features from tiny images. 2009.

Yann LeCun, Léon Bottou, Yoshua Bengio, and Patrick Haffner. Gradient-based learning applied to document recognition. *Proceedings of the IEEE*, 86(11):2278–2324, 1998.

Doyup Lee, Sungwoong Kim, Ildoo Kim, Yeongjae Cheon, Minsu Cho, and Wook-Shin Han. Contrastive regularization for semi-supervised learning. In *Proceedings of the IEEE/CVF Conference on Computer Vision and Pattern Recognition*, pp. 3911–3920, 2022.

Jason D Lee, Qi Lei, Nikunj Saunshi, and Jiacheng Zhuo. Predicting what you already know helps: Provable self-supervised learning. *Advances in Neural Information Processing Systems*, 34:309–323, 2021.

Hong Liu, Jeff Z HaoChen, Adrien Gaidon, and Tengyu Ma. Self-supervised learning is more robust to dataset imbalance. In *NeurIPS 2021 Workshop on Distribution Shifts: Connecting Methods and Applications*, 2021.

Ilya Loshchilov and Frank Hutter. Decoupled weight decay regularization. In *International Conference on Learning Representations*, 2018.

Kaili Ma, Haochen Yang, Han Yang, Tatiana Jin, Pengfei Chen, Yongqiang Chen, Barakeel Fanseu Kamhoua, and James Cheng. Improving graph representation learning by contrastive regularization. *arXiv preprint arXiv:2101.11525*, 2021.

Andrew L. Maas, Raymond E. Daly, Peter T. Pham, Dan Huang, Andrew Y. Ng, and Christopher Potts. Learning word vectors for sentiment analysis. In *Proceedings of the 49th Annual Meeting of the Association for Computational Linguistics: Human Language Technologies*, pp. 142–150, Portland, Oregon, USA, June 2011. Association for Computational Linguistics. URL http://www.aclweb.org/anthology/P11-1015.

Yuval Netzer, Tao Wang, Adam Coates, Alessandro Bissacco, Bo Wu, and Andrew Y Ng. Reading digits in natural images with unsupervised feature learning. 2011.

Alejandro Newell and Jia Deng. How useful is self-supervised pretraining for visual tasks? In *2020 IEEE/CVF Conference on Computer Vision and Pattern Recognition, CVPR 2020, Seattle, WA, USA, June 13-19, 2020*, pp. 7343–7352. Computer Vision Foundation / IEEE, 2020. doi: 10.1109/CVPR42600.2020.00737. URL https://openaccess.thecvf.com/content_CVPR_2020/html/Newell_How_Useful_Is_Self-Supervised_Pretraining_for_Visual_Tasks_CVPR_2020_paper.html.

Hong-Wei Ng and Stefan Winkler. A data-driven approach to cleaning large face datasets. In *2014 IEEE international conference on image processing (ICIP)*, pp. 343–347. IEEE, 2014.

B. Olshausen and D. Field. Sparse coding with an overcomplete basis set: A strategy employed by v1? *Vision Research*, 37:3311–3325, 1997.

Karl Pearson. LIII. On lines and planes of closest fit to systems of points in space. *The London, Edinburgh, and Dublin philosophical magazine and journal of science*, 2(11):559–572, 1901.

Alec Radford, Jong Wook Kim, Chris Hallacy, Aditya Ramesh, Gabriel Goh, Sandhini Agarwal, Girish Sastry, Amanda Askell, Pamela Mishkin, Jack Clark, Gretchen Krueger, and Ilya Sutskever. Learning transferable visual models from natural language supervision. In *Proceedings of the 38th International Conference on Machine Learning, ICML 2021, 18-24 July 2021, Virtual Event*, volume 139 of *Proceedings of Machine Learning Research*, pp. 8748–8763. PMLR, 2021. URL http://proceedings.mlr.press/v139/radford21a.html.

Aditya Ramesh, Prafulla Dhariwal, Alex Nichol, Casey Chu, and Mark Chen. Hierarchical text-conditional image generation with clip latents. *arXiv preprint arXiv:2204.06125*, 2022.

Nikunj Saunshi, Jordan Ash, Surbhi Goel, Dipendra Misra, Cyril Zhang, Sanjeev Arora, Sham Kakade, and Akshay Krishnamurthy. Understanding contrastive learning requires incorporating inductive biases. *arXiv preprint arXiv:2202.14037*, 2022a.

Nikunj Saunshi, Jordan Ash, Surbhi Goel, Dipendra Misra, Cyril Zhang, Sanjeev Arora, Sham Kakade, and Akshay Krishnamurthy. Understanding contrastive learning requires incorporating inductive biases. In Kamalika Chaudhuri, Stefanie Jegelka, Le Song, Csaba Szepesvari, Gang Niu, and Sivan Sabato (eds.), *Proceedings of the 39th International Conference on Machine Learning*, volume 162 of *Proceedings of Machine Learning Research*, pp. 19250–19286. PMLR, 17–23 Jul 2022b. URL https://proceedings.mlr.press/v162/saunshi22a.html.

Kendrick Shen, Robbie M Jones, Ananya Kumar, Sang Michael Xie, Jeff Z HaoChen, Tengyu Ma, and Percy Liang. Connect, not collapse: Explaining contrastive learning for unsupervised domain adaptation. In *International Conference on Machine Learning*, pp. 19847–19878. PMLR, 2022.

Zhenmei Shi, Junyi Wei, and Yingyu Liang. A theoretical analysis on feature learning in neural networks: Emergence from inputs and advantage over fixed features. In *International Conference on Learning Representations*, 2022.

Johannes Stallkamp, Marc Schlipsing, Jan Salmen, and Christian Igel. Man vs. computer: Benchmarking machine learning algorithms for traffic sign recognition. *Neural Networks*, 32:323–332, 2012. doi: 10.1016/j.neunet.2012.02.016. URL https://doi.org/10.1016/j.neunet.2012.02.016.

Yi-Lin Sung, Jaemin Cho, and Mohit Bansal. Vl-adapter: Parameter-efficient transfer learning for vision-and-language tasks. In *Proceedings of the IEEE/CVF Conference on Computer Vision and Pattern Recognition*, pp. 5227–5237, 2022.

Yuandong Tian. Deep contrastive learning is provably (almost) principal component analysis. *arXiv preprint arXiv:2201.12680*, 2022.

Christopher Tosh, Akshay Krishnamurthy, and Daniel Hsu. Contrastive learning, multi-view redundancy, and linear models. In *Algorithmic Learning Theory*, pp. 1179–1206. PMLR, 2021.

Yao-Hung Hubert Tsai, Yue Wu, Ruslan Salakhutdinov, and Louis-Philippe Morency. Self-supervised learning from a multi-view perspective. In *International Conference on Learning Representations*, 2020.

Aäron van den Oord, Yazhe Li, and Oriol Vinyals. Representation learning with contrastive predictive coding. *CoRR*, abs/1807.03748, 2018. URL `http://arxiv.org/abs/1807.03748`.

Laurens Van der Maaten and Geoffrey Hinton. Visualizing data using t-sne. *Journal of machine learning research*, 9(11), 2008.

Wouter Van Gansbeke, Simon Vandenhende, Stamatios Georgoulis, and Luc V Gool. Revisiting contrastive methods for unsupervised learning of visual representations. *Advances in Neural Information Processing Systems*, 34:16238–16250, 2021.

Tongzhou Wang and Phillip Isola. Understanding contrastive representation learning through alignment and uniformity on the hypersphere. In *International Conference on Machine Learning*, pp. 9929–9939. PMLR, 2020.

Zixin Wen and Yuanzhi Li. Toward understanding the feature learning process of self-supervised contrastive learning. In *International Conference on Machine Learning*, pp. 11112–11122. PMLR, 2021.

Han Xiao, Kashif Rasul, and Roland Vollgraf. Fashion-mnist: a novel image dataset for benchmarking machine learning algorithms. *arXiv preprint arXiv:1708.07747*, 2017.

Xingyi Yang, Xuehai He, Yuxiao Liang, Yue Yang, Shanghang Zhang, and Pengtao Xie. Transfer learning or self-supervised learning? A tale of two pretraining paradigms. *CoRR*, abs/2007.04234, 2020. URL `https://arxiv.org/abs/2007.04234`.

Jure Zbontar, Li Jing, Ishan Misra, Yann LeCun, and Stéphane Deny. Barlow twins: Self-supervised learning via redundancy reduction. In *Proceedings of the 38th International Conference on Machine Learning, ICML 2021, 18-24 July 2021, Virtual Event*, volume 139 of *Proceedings of Machine Learning Research*, pp. 12310–12320. PMLR, 2021. URL `http://proceedings.mlr.press/v139/zbontar21a.html`.

Xiang Zhang, Junbo Jake Zhao, and Yann LeCun. Character-level convolutional networks for text classification. In *NIPS*, 2015.

Roland S Zimmermann, Yash Sharma, Steffen Schneider, Matthias Bethge, and Wieland Brendel. Contrastive learning inverts the data generating process. In *International Conference on Machine Learning*, pp. 12979–12990. PMLR, 2021.

Appendix

A PROOFS FOR SECTION 2.1

Theorem A.1 (Restatement of Theorem 2.1)**.** *If $\ell(t) = -t$, then the contrastive loss is equivalent to the PCA objective on ϕ_{z_R}:*

$$\mathbb{E}\left[\ell\left(\phi(x)^\top[\phi(x^+) - \phi(x^-)]\right)\right] = -\mathbb{E}\left[\|\phi_{z_R} - \phi_0\|^2\right]. \tag{10}$$

If additionally $\phi(x)$ is linear in x, then the contrastive loss is equivalent to the linear PCA objective on data from the distribution $p_{\bar{x}}$ of $\bar{x} = \mathbb{E}_{z_U}[x]$:

$$\mathbb{E}\left[\ell\left(\phi(x)^\top[\phi(x^+) - \phi(x^-)]\right)\right] = -\mathbb{E}\left[\|\phi(\bar{x}) - \phi_0\|^2\right]. \tag{11}$$

Proof. We first present some preliminaries for the proof. Recall that in our hidden representation data model $x = g(z)$. The learned representation is $\phi(x) = \phi(g(z)) = \phi \circ g(z)$. For brevity, let us define $\phi(x) = \phi \circ g(z) := h(z)$. Also, the hidden representations corresponding to (x, x^+, x^-) are given by (z, z^+, z^-), where

$$z = [z_R\,;\, z_U], \;\; z^+ = [z_R\,;\, z_U^+], \;\; z^- = [z_R^-\,;\, z_U^-],$$

where z_R and z_R^- are sampled independently from the distribution $\mathcal{D}_R$; and z_U, z_U^+, and z_U^- are sampled independently from the distribution $\mathcal{D}_U$. The expectation of an arbitrary function $f(z, z^+, z^-)$ can be simplified as follows:

$$\begin{aligned}\mathbb{E}_{(z,z^+,z^-)}\left[f(z, z^+, z^-)\right] &= \mathbb{E}_{(z_R,z_R^-,z_U,z_U^+,z_U^-)}\left[f(z, z^+, z^-)\right] \\ &= \mathbb{E}_{(z_R,z_R^-)}\left[\mathbb{E}_{(z_U,z_U^+,z_U^-)}\left[f(z, z^+, z^-) \mid z_R, z_R^-\right]\right].\end{aligned}$$

The second step follows from the law of iterated expectations.

The negative expected contrastive loss is

$$\begin{aligned}
&-\mathbb{E}_{(x,x^+,x^-)}\left[\,\ell\left(\phi(x)^\top[\phi(x^+) - \phi(x^-)]\right)\right] && (12)\\
&= -\mathbb{E}_{(z,z^+,z^-)}\left[\,\ell\left(\phi(g(z))^\top[\phi(g(z^+)) - \phi(g(z^-))]\right)\right] && (13)\\
&= \mathbb{E}_{(z,z^+,z^-)}\left[\,h(z)^\top[h(z^+) - h(z^-)]\,\right] && (14)\\
&= \mathbb{E}_{(z_R,z_R^-)}\left[\,\mathbb{E}\left[\,h(z)^\top[h(z^+) - h(z^-)] \mid z_R, z_R^-\,\right]\right] && (15)\\
&= \mathbb{E}_{(z_R,z_R^-)}\left[\mathbb{E}\left[h(z) \mid z_R\right]^\top\left(\mathbb{E}\left[h(z^+) \mid z_R\right] - \mathbb{E}\left[h(z^-) \mid z_R^-\right]\right)\right] && (16)\\
&= \mathbb{E}_{(z_R,z_R^-)}\left[\mathbb{E}\left[\phi(x) \mid z_R\right]^\top\left(\mathbb{E}\left[\phi(x^+) \mid z_R\right] - \mathbb{E}\left[\phi(x^-) \mid z_R^-\right]\right)\right] && (17)\\
&= \mathbb{E}_{(z_R,z_R^-)}\left[\phi_{z_R}^\top\left(\phi_{z_R} - \phi_{z_R^-}\right)\right]. && (18)
\end{aligned}$$

The second equality follows from the choice of loss $\ell(t) = -t$, and the fourth equality follows from the fact that z_U, z_U^+, and z_U^- are sampled independently from the distribution $\mathcal{D}_U$. Also, we have defined $\phi_{z_R} := \mathbb{E}\left[\phi(x) \mid z_R\right]$.

Denote the centered representation as $\bar{\phi}_{z_R} = \phi_{z_R} - \phi_0$. Then we have

$$\begin{aligned}
&-\mathbb{E}_{(x,x^+,x^-)}\left[\ell\left(\phi(x)^\top[\phi(x^+) - \phi(x^-)]\right)\right] && (19)\\
&= \mathbb{E}_{(z_R,z_R^-)}\left[\phi_{z_R}^\top\left(\phi_{z_R} - \phi_{z_R^-}\right)\right] && (20)\\
&= \mathbb{E}_{(z_R,z_R^-)}\left[(\bar{\phi}_{z_R} + \phi_0)^\top\left(\bar{\phi}_{z_R} + \phi_0 - \bar{\phi}_{z_R^-} - \phi_0\right)\right] && (21)\\
&= \mathbb{E}_{(z_R,z_R^-)}\left[(\bar{\phi}_{z_R} + \phi_0)^\top\left(\bar{\phi}_{z_R} - \bar{\phi}_{z_R^-}\right)\right] && (22)\\
&= \mathbb{E}_{(z_R,z_R^-)}\left[\bar{\phi}_{z_R}^\top\bar{\phi}_{z_R} - \bar{\phi}_{z_R}^\top\bar{\phi}_{z_R^-}\right] + \mathbb{E}_{(z_R,z_R^-)}\left[\phi_0^\top\left(\bar{\phi}_{z_R} - \bar{\phi}_{z_R^-}\right)\right]. && (23)
\end{aligned}$$

Since $\bar{\phi}_{z_R}$ and $\bar{\phi}_{z_R^-}$ are independent with mean 0, we have $\mathbb{E}_{(z_R,z_R^-)}[\bar{\phi}_{z_R}^\top \bar{\phi}_{z_R^-}] = 0$, $\mathbb{E}_{(z_R,z_R^-)}[\phi_0^\top \bar{\phi}_{z_R}] = 0$, and $\mathbb{E}_{(z_R,z_R^-)}[\phi_0^\top \bar{\phi}_{z_R^-}] = 0$. Therefore,

$$
\begin{aligned}
&-\mathbb{E}_{(x,x^+,x^-)}\left[\ell\left(\phi(x)^\top[\phi(x^+)-\phi(x^-)]\right)\right] && (24)\\
&= \mathbb{E}_{z_R}\left[\bar{\phi}_{z_R}^\top \bar{\phi}_{z_R}\right] && (25)\\
&= \mathbb{E}_{z_R}\left[\|\bar{\phi}_{z_R}\|^2\right] && (26)\\
&= \mathbb{E}_{z_R}\left[\|\phi_{z_R}-\phi_0\|^2\right], && (27)
\end{aligned}
$$

which is the PCA objective on the mean representation ϕ_{z_R}.

If additionally $\phi(x)$ is linear in x, then

$$
\begin{aligned}
&-\mathbb{E}_{(x,x^+,x^-)}\left[\ell\left(\phi(x)^\top[\phi(x^+)-\phi(x^-)]\right)\right] && (28)\\
&= \mathbb{E}_{z_R}\left[\|\phi_{z_R}-\phi_0\|^2\right] && (29)\\
&= \mathbb{E}_{\bar{x}}\left[\|\phi(\bar{x})-\phi(x_0)\|^2\right] && (30)
\end{aligned}
$$

which is the linear PCA objective on the data from the distribution of $\bar{x} = \mathbb{E}[x|z_R]$. □

Theorem A.2 (Restatement of Theorem 2.2)**.** *Under Assumptions **(A1)(A2)(A3)**:*

(1) The optimal representation ϕ^* does not encode z_U: $\phi^* \circ g(z)$ is independent of z_U.

(2) For any invariant feature $i \in R$, there exists $B_i > 0$ such that as long as the representations' norm $B_r \geq B_i$, the optimal representation encodes z_i. Furthermore, if z_R is discrete, then B_i is monotonically decreasing in $\Pr[z_{R\setminus\{i\}} = z_{R\setminus\{i\}}^-, z_i \neq z_i^-]$, the probability that in z_R and z_R^-, the i-th feature varies while the others remain the same.

Proof. (1) Recall that

$$
\phi_{z_R} = \mathbb{E}[\phi \circ g(z) \mid z_R], \quad \phi_0 = \mathbb{E}_z[\phi \circ g(z)] = \mathbb{E}_{z_R}[\phi_{z_R}]. \tag{31}
$$

Then the contrastive loss at pre-training is:

$$
\begin{aligned}
&\mathbb{E}_{(x,x^+,x^-)}\left[\ell\left(\phi(x)^\top[\phi(x^+)-\phi(x^-)]\right)\right] && (32)\\
&= \mathbb{E}_{(z,z^+,z^-)}\left[\ell\left((\phi\circ g(z))^\top(\phi\circ g(z^+)-\phi\circ g(z^-))\right)\right] && (33)\\
&= \mathbb{E}_{(z_R,z_R^-)}\left[\mathbb{E}\left[\ell\left((\phi\circ g(z))^\top(\phi\circ g(z^+)-\phi\circ g(z^-))\right) \mid z_R, z_R^-\right]\right] && (34)\\
&\geq \mathbb{E}_{(z_R,z_R^-)}\left[\ell\left(\mathbb{E}\left[(\phi\circ g(z))^\top(\phi\circ g(z^+)-\phi\circ g(z^-)) \mid z_R, z_R^-\right]\right)\right] && (35)\\
&= \mathbb{E}_{(z_R,z_R^-)}\left[\ell\left(\mathbb{E}[\phi\circ g(z) \mid z_R]^\top\left(\mathbb{E}[\phi\circ g(z^+) \mid z_R]-\mathbb{E}[\phi\circ g(z^-) \mid z_R^-]\right)\right)\right] && (36)\\
&= \mathbb{E}_{(z_R,z_R^-)}\left[\ell\left(\phi_{z_R}^\top\phi_{z_R}-\phi_{z_R}^\top\phi_{z_R^-}\right)\right], && (37)
\end{aligned}
$$

where the inequality comes from the convexity of $\ell(z)$ and Jensen's inequality applied to the inner expectation. The inequality becomes equality when the representation function ϕ is invariant to the spurious features z_U, i.e., with probability 1 over the distribution, $\phi \circ g(z) = \phi_{z_R}$. Therefore, the spurious features z_U are not encoded in the optimal representation, proving the first part.

(2) First consider the case when z has discrete values from a finite set. When the generative function $g(z)$ is not independent of z_i, we assume for contradiction that the optimal representation ϕ is independent of z_i. From (1), we know that it is independent of z_U. So there exists an f such that $\phi \circ g(z) = f(z_{R\setminus\{i\}})$. Without loss of generality, suppose $U = \emptyset$, then $\phi \circ g(z) = f(z_{-i})$.

Since the generative function $g(z)$ is not independent of z_i, there exist z and z^-, such that $z_{-i} = z_{-i}^-$, $z_i \neq z_i^-$, $g(z) \neq g(z^-)$, and z, z^- have non-zero probabilities. So $\Pr[z_{-i} = z_{-i}^-, z_i \neq z_i^-] > 0$.

Now construct a new representation function $\bar{\phi} \in \mathbb{R}^{k+n}, n = |\mathcal{Z}|$ such that $\bar{\phi} \circ g(z) = h(z)$ as follows :

$$
h(z) = \left[\sqrt{1-\alpha^2}f(z_{-i}), \quad \alpha\|f(z_{-i})\|\mathbf{I}_z\right] \tag{38}
$$

where $\mathbf{I}_z$ is the one-hot encoding of the value z. Note that $\bar{\phi}$ still satisfies that norm bound since $\|\bar{\phi}(x)\| = \|h(z)\| = \|f(z_{-i})\|$. We next show that the contrastive loss of $\bar{\phi}$ can be smaller than that of ϕ, leading to a contradiction and finishing the proof.

The contrastive loss of $\bar{\phi}$ (using the fact that $z^+ = z$ when $U = \emptyset$) is

$$\mathbb{E}_{(z,z^-)}\left[\ell\left(h(z)^\top h(z) - h(z)^\top h(z^-)\right)\right] \tag{39}$$

$$= \mathbb{E}_{(z,z^-)}\left[\ell\left(h(z)^\top h(z) - h(z)^\top h(z^-)\right) \mid z \neq z^-\right] \Pr[z \neq z^-] \; + \; \mathbb{E}_{z,z^-}\left[\ell(0)\right] \Pr[z = z^-]. \tag{40}$$

We only need to consider the first term.

$$\mathbb{E}_{(z,z^-)}\left[\ell\left(h(z)^\top h(z) - h(z)^\top h(z^-)\right) \mid z \neq z^-\right] \Pr[z \neq z^-] \tag{41}$$

$$= \mathbb{E}_{(z,z^-)}\Big[\underbrace{\ell\left(\|f(z_{-i})\|^2 - (1-\alpha^2) f(z_{-i})^\top f(z_{-i}^-)\right)}_{T_1} \mid z_{-i} \neq z_{-i}^-\Big] \Pr[z_{-i} \neq z_{-i}^-] \tag{42}$$

$$+ \; \mathbb{E}_{(z,z^-)}\Big[\underbrace{\ell\left(\alpha^2 \|f(z_{-i})\|^2\right)}_{T_2} \mid z_{-i} = z_{-i}^-,\, z_i \neq z_i^-\Big] \Pr[z_{-i} = z_{-i}^-,\, z_i \neq z_i^-]. \tag{43}$$

When $\alpha = 0$, the above reduce to the corresponding terms for ϕ, so we would like to show that there exists non-zero α that leads to smaller loss values.

Recall that $\ell(\cdot)$ is decreasing by property (A3). Let $\alpha = \sqrt{1/2}/B_r$, where $B_r = \|f(z_{-i})\|$. Then when switching from ϕ to $\bar{\phi}$, T_2 goes from $\ell(0)$ to $\ell(1/2)$, a constant reduction. For T_1, if $f(z_{-i})^\top f(z_{-i}^-)$ is positive, then T_1 decreases; if $f(z_{-i})^\top f(z_{-i}^-)$ is negative, then T_1 increases from $\ell(B_r^2 - f(z_{-i})^\top f(z_{-i}^-))$ to $\ell(B_r^2 - f(z_{-i})^\top f(z_{-i}^-) + \alpha^2 f(z_{-i})^\top f(z_{-i}^-))$. Note that $|\alpha^2 f(z_{-i})^\top f(z_{-i}^-)| \leq 1$ (by the Cauchy-Schwarz inequality); so the increase in T_1 diminishes when B_r grows, by the property (A3) of ℓ. Then when B_r is large enough, the increase in T_1 is smaller than the decrease in T_2. So from ϕ to $\bar{\phi}$, the contrastive loss decreases, contradicting that ϕ is optimal. Finally, since the reduction in (43) is smaller when $\Pr[z_{-i} = z_{-i}^-, z_i \neq z_i^-]$ is smaller, then B_i needs to be larger. So B_i is monotonically decreasing in $\Pr[z_{-i} = z_{-i}^-, z_i \neq z_i^-]$.

Now consider the general case when z may not be from a finite set. For any $\epsilon_0 > 0$, there exists a ℓ_2 ball $\mathcal{B}$ of bounded radius such that the probability of z outside the ball is at most ϵ_0. Since $\phi \circ g$'s are regular by assumption, there exists a partition $\mathcal{Z} \cap \mathcal{B}$ into finitely many subsets such that in each subset and for each $\phi \circ g$, the function value varies by at most ϵ_0. Construct a new distribution $\mathcal{D}_z'$ for z: select a representative point in each subset, and put a probability mass to it equal to that of the original distribution $\mathcal{D}_z$ in this subset, and normalize the probabilities over the subsets. The new distribution is over a finite set so the above argument holds. Furthermore, the difference in the T_1 term for $\mathcal{D}_z'$ and $\mathcal{D}_z$ can be made arbitrarily small by choosing sufficiently small ϵ_0; similarly for T_2. Then the argument also holds for $\mathcal{D}_z$, which completes the proof for the general case. □

A.1 Inductive Biases are Needed for Analyzing Prediction Success

We have analyzed what features are encoded in the representation. However, encoding the information does not equate to good prediction performance, in particular, with linear predictors. Recently, Saunshi et al. (2022b) demonstrated that existing analyses that ignore the inductive biases of the model and algorithm cannot adequately explain the prediction success, and provided examples where such analysis can lead to vacuous bounds. One may wonder if our hidden representation data model can provide inductive biases that avoid such vacuous bounds. Unfortunately, similar issues as in Saunshi et al. (2022b) remain.

To illustrate that inductive biases are still needed in our data model, consider the following simple example. Suppose $z_R \in \{-1, 1\}^2$ and can be recovered from x; the label y is simply the first coordinate in z_R. Suppose the representation satisfies $\phi(x) \in \mathbb{R}^2, \|\phi(x)\| = 1$, and contrastive learning uses the logistic loss $\ell(z)$. Let $\phi(x)$ be such that $\phi \circ g(z) = h(z_R)$, and $h((-1,-1)) = (-1, 0), h((-1,1)) = (1,0), h((1,-1)) = (0,-1), h((1,1)) = (0,1)$. It can be verified that this ϕ is optimal for the contrastive loss. However, on the representation ϕ, the classification is an XOR-problem (Fig. 6), for which there is no non-trivial error bound for linear predictors. This contradicts the success of linear probing in practice.

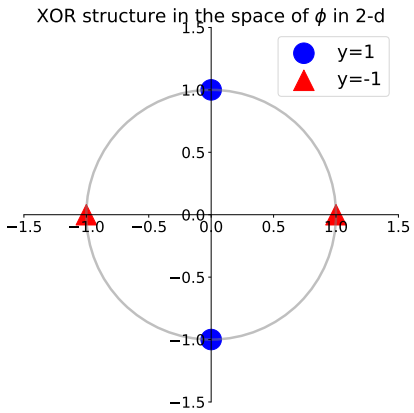

Figure 6: A two-dim example of XOR structure in the space of ϕ.

Furthermore, some restrictions on the data distributions are also needed. Suppose *all* optimal representations are linearly separable with certain inductive biases on the representation function class. Suppose the label y depends on z_R. Without restrictions on the labeling function, one can consider a random $y \in \{-1, +1\}$ over any z_R. Then for any linear predictor on any optimal representation, in expectation the error is $1/2$, so there is always a labeling function for which no non-trivial error can be achieved. Our analysis thus requires restrictions on the dependence of the label on z_R (in particular, linear dependence).

B Proofs and More Analysis for Section 2.2

B.1 Lemmas for a more general setting

We will prove the results in a more general setting, where the mixture can be uneven and the variances of different types of features can be different. The results in Section 2.2 then follow from these lemmas.

In the more general setting, the diverse pre-training data is a mixture of data from T different tasks $\mathcal{D}_t$'s, while the target task is one of the tasks. In the mixture, the task $\mathcal{D}_t$ has weight $w_t > 0$ and $\sum_{t=1}^{T} w_t = 1$. All tasks share a public feature set S of size s, and each task $\mathcal{D}_t$ additionally owns a private disjoint feature set P_t of size $r - s$, i.e., $P_t \cap S = \emptyset$ for $t \in [T]$ and $P_{t_1} \cap P_{t_2} = \emptyset$ for $t_1 \neq t_2$. The invariant features for $\mathcal{D}_t$ are then $R_t = S \cup P_t$. All invariant features are $\cup_{t=1}^{T} R_t \subseteq R$, $k := |R|$, and spurious features are $U = [d] \setminus R$. In task $\mathcal{D}_t$, the positive pairs (x, x^+) are generated as follows:

$$z_S \sim \mathcal{N}(0, \sigma_{S,t}^2 I), z_{P_t} \sim \mathcal{N}(0, \sigma_{R,t}^2 I), z_{R \setminus R_t} = 0, \tag{44}$$

$$z_U \sim \mathcal{N}(0, \sigma_{U,t}^2 I), z = [z_R; z_U], \quad x = g(z), \tag{45}$$

$$z_U^+ \sim \mathcal{N}(0, \sigma_{U,t}^2 I), z^+ = [z_R; z_U^+], \quad x^+ = g(z^+), \tag{46}$$

and x^- is simply an i.i.d. copy from the same distribution as x. In practice, multiple independent negative examples are used, and thus we consider the following contrastive loss

$$\min_{\phi \in \Phi} \mathbb{E}_{(x, x^+)} \left[\ell \left(\phi(x)^\top (\phi(x^+) - \mathbb{E}_{x^-} \phi(x^-)) \right) \right] \tag{47}$$

to pre-train a representation ϕ. Then, when using ϕ for prediction in the target task $\mathcal{D}_t$, the predictor class should contain a predictor matching the ground-truth label, so consider the class:

$$\mathcal{F}_{\phi,t} = \{ f(z) = u_t^\top z : u_t \in \mathbb{R}^k, \|u_t\| \leq B_{\phi,t} \} \tag{48}$$

where $B_{\phi,t}$ is the minimum value such that there exists $u_t \in \mathcal{F}_{\phi,t}$ with $y = u_t^\top \phi(x)$ on $\mathcal{D}_t$.

Recall that we assume a linear data model and linear representation functions ϕ:

- x is linear in z: $x = g(z) = Mz$ where $M \in \mathbb{R}^{d\times d}$ is an orthonormal dictionary. The label in task $\mathcal{D}_t$ is linear in its invariant features $y = (u_t^*)^\top z_{R_t}$ for some $u_t^* \in \mathbb{R}^r$.
- The representations are linear functions with weights of bounded spectral/Frobenius norms:

$$\Phi = \{\phi(x) = Wx : W\in\mathbb{R}^{k\times d}, \|W\|\leq 1, \|W\|_F\leq\sqrt{r}\}.$$

  Here the norm bounds are chosen to be the minimum values to allow recovering the invariant features in the target task, i.e., there exists $\phi \in \Phi$ such that $\phi(x) = [z_{R_t}; \mathbf{0}]$.

Lemma B.1. *Consider the above setting. Let $\alpha, \alpha_t (t \in [T])$ be the optimizer for*

$$\min_{\tilde{\alpha},\tilde{\alpha}_1,\ldots,\tilde{\alpha}_T} \sum_{t=1}^{T} w_t \mathbb{E}\left[\ell\left(\tilde{\alpha}\sigma_{S,t}^2 Z + \tilde{\alpha}_t \sigma_{R,t}^2 Z_t\right)\right], \tag{49}$$

$$\textit{subject to} \quad \tilde{\alpha}s + \sum_{t=1}^{T} \tilde{\alpha}_t (r-s) \leq r, \tag{50}$$

$$\tilde{\alpha}, \tilde{\alpha}_t \in [0,1], \tag{51}$$

where $Z \sim \chi_s^2$ and $Z_t \sim \chi_{r-s}^2$.

Then the optimal representation $\phi^*(x)$ the loss (47) in contrastive learning satisfies $\phi^*(x) = W^*x$ with any W^* of the form:

$$W^* = [QA^*, \boldsymbol{0}]M^{-1} \tag{52}$$

where $Q \in \mathbb{R}^{k\times k}$ is any orthonormal matrices, A^* is a $k \times k$ diagonal matrix with

$$A_{jj}^* = \begin{cases} \sqrt{\alpha} & \text{if } j \in S, \\ \sqrt{\alpha_t} & \text{if } j \in P_t, \\ 0 & \text{otherwise,} \end{cases} \tag{53}$$

and the matrix of zeros has size $k \times (d-k)$.

Proof. For each $\mathcal{D}_t$,

$$\begin{aligned}
&\mathbb{E}_{(x,x^+)}\left[\ell\left(\phi(x)^\top[\phi(x^+) - \mathbb{E}_{x^-}\phi(x^-)]\right)\right] && (54)\\
&= \mathbb{E}_{(z,z^+)}\left[\ell\left((WMz)^\top(WMz^+ - \mathbb{E}_{z^-}[WMz^-])\right)\right] && (55)\\
&= \mathbb{E}_{(z,z^+)}\left[\ell\left(z^\top(M^\top W^\top WM)(z^+ - \mathbb{E}_{z^-}[z^-])\right)\right] && (56)\\
&\geq \mathbb{E}_{z_R}\left[\ell\left((\mathbb{E}_{z_U}[z])^\top M^\top W^\top WM(\mathbb{E}_{z_U^+}[z^+] - \mathbb{E}_{z^-}[z^-])\right)\right] && (57)\\
&= \mathbb{E}_{z_R}\left[\ell\left([z_R;\mathbf{0}]^\top M^\top W^\top WM([z_R;\mathbf{0}] - 0)\right)\right] && (58)\\
&= \mathbb{E}_{z_R}\left[\ell\left(\|WM[z_R;\mathbf{0}]\|^2\right)\right] && (59)
\end{aligned}$$

where the inequality comes from the convexity of $\ell(t)$ and Jensen's inequality. Similar to Theorem 2.2, the equality holds iff WMz does not depend on z_U and WMz^+ does not depend on z_U^+, so the optimal solution should satisfy this condition.

Let $WM = [A_R, A_U]$ where $A_R \in \mathbb{R}^{k\times k}, A_U \in \mathbb{R}^{k\times(d-k)}$. By rotational invariance of z_S, and z_{P_t}, without loss of generality, we can assume $A_R = QA$ where A is a diagonal matrix with diagonal entries a_{jj}'s and Q is any orthonormal matrix. Furthermore, $A_U = 0$ in the optimal solution since it does not affect the loss but only decreases the norm bound on A_R. So on data from the task $\mathcal{D}_t$,

$$\mathbb{E}_{\mathcal{D}_t}\left[\ell\left(\|WM[z_R;\mathbf{0}]\|^2\right)\right] = \mathbb{E}_{z_{R_t}}\left[\ell\left(\sum_{j\in R_t} a_{jj}^2 z_j^2\right)\right]. \tag{60}$$

Then on the mixture,

$$\mathbb{E}_{(x,x^+)}\left[\ell\left(\phi(x)^\top[\phi(x^+)-\mathbb{E}_{x^-}\phi(x^-)]\right)\right] \tag{61}$$

$$\geq \sum_{t=1}^{T} w_t \mathbb{E}_{\{z_j\}}\left[\ell\left(\sum_{j\in R_t} a_{jj}^2 z_j^2\right)\right] \tag{62}$$

$$= \sum_{t=1}^{T} w_t \mathbb{E}_{\{\tilde{z}_j\sim\mathcal{N}(0,1)\}}\left[\ell\left(\sum_{j\in S} a_{jj}^2\sigma_{S,t}^2\tilde{z}_j^2 + \sum_{j\in P_t} a_{jj}^2\sigma_{R,t}^2\tilde{z}_j^2\right)\right] \tag{63}$$

$$:= g(\{a_{jj}\}), \tag{64}$$

where each $\tilde{z}_j$ is a random variable drawn from standard Gaussian.

Now consider the minimum of the function $g(\{a_{jj}\})$ on the right hand side, under the constraints that $|a_{jj}| \leq 1$ and $\sum_j a_{jj}^2 \leq r$. Before finishing the proof of Lemma B.1, we have the following claim for this optimization.

Claim 1. *There exist α, α_t satisfying $0 \leq \alpha, \alpha_t \leq 1$ and $\alpha s + \sum_{t=1}^{T}\alpha_t(r-s) = \sum_j a_{jj}^2 \leq r$, such that the minimum of the above optimization (64) is achieved when $a_{jj}^2 = \alpha$ for any $j \in S$, and $a_{jj}^2 = \alpha_t$ for any $j \in P_t$ and $t \in [T]$.*

Proof. We need to prove that to achieve the minimum,

(1) $a_{\ell\ell}^2 = a_{\ell'\ell'}^2$ for any $\ell \neq \ell' \in S$;

(2) $a_{\ell\ell}^2 = a_{\ell'\ell'}^2$ for any $\ell \neq \ell' \in P_t$ and any $t \in [T]$;

For (1): By symmetry of z_j's and the convexity of $\ell(\cdot)$, for any $t \in [T]$,

$$\mathbb{E}\left[\ell\left(\sum_{j\in R_t} a_{jj}^2 z_j^2\right)\right] \tag{65}$$

$$= \frac{1}{2}\mathbb{E}\left[\ell\left(\sum_{j\in S, j\neq\ell, j\neq\ell'} a_{jj}^2 z_j^2 + a_{\ell\ell}^2 z_\ell^2 + a_{\ell'\ell'}^2 z_{\ell'}^2 + \sum_{j\in P_t} a_{jj}^2 z_j^2\right)\right] \tag{66}$$

$$+ \frac{1}{2}\mathbb{E}\left[\ell\left(\sum_{j\in S, j\neq\ell, j\neq\ell'} a_{jj}^2 z_j^2 + a_{\ell\ell}^2 z_{\ell'}^2 + a_{\ell'\ell'}^2 z_\ell^2 + \sum_{j\in P_t} a_{jj}^2 z_j^2\right)\right] \tag{67}$$

$$\geq \mathbb{E}\left[\ell\left(\sum_{j\in S, j\neq\ell, j\neq\ell'} a_{jj}^2 z_j^2 + \frac{a_{\ell\ell}^2 + a_{\ell'\ell'}^2}{2} z_{\ell'}^2 + \frac{a_{\ell\ell}^2 + a_{\ell'\ell'}^2}{2} z_\ell^2 + \sum_{j\in P_t} a_{jj}^2 z_j^2\right)\right]. \tag{68}$$

Then

$$g(\{a_{jj}\}) \geq \sum_{t=1}^{T} w_t \mathbb{E}\left[\ell\left(\sum_{j\in S, j\neq\ell, j\neq\ell'} a_{jj}^2 z_j^2 + \frac{a_{\ell\ell}^2 + a_{\ell'\ell'}^2}{2} z_{\ell'}^2 + \frac{a_{\ell\ell}^2 + a_{\ell'\ell'}^2}{2} z_\ell^2 + \sum_{j\in P_t} a_{jj}^2 z_j^2\right)\right]. \tag{69}$$

Therefore, the minimum is achieved when $a_{\ell\ell}^2 = a_{\ell'\ell'}^2$.

A similar argument as above proves statement (2). □

These statements mean that, for any $t \in [T]$, the minimum is achieved when $a_{jj}^2 = \alpha$ for $j \in S$, and $a_{jj}^2 = \alpha_t$ for $j \in P_t$, for some values $\alpha, \alpha_t \geq 0$. Let $Z = \sum_{j\in S}\tilde{z}_j^2, Z_t = \sum_{j\in P_t}\tilde{z}_j^2$. Then $Z \sim \chi_s^2$

and $Z_t \sim \chi^2_{r-s}$, and we have:

$$g(\{a_{jj}\}) = \sum_{t=1}^{T} w_t \mathbb{E}\left[\ell\left(\sum_{j\in S} \alpha\sigma^2_{S,t}\tilde{z}_j^2 + \sum_{j\in P_t} \alpha_t\sigma^2_{R,t}\tilde{z}_j^2\right)\right] \tag{70}$$

$$= \sum_{t=1}^{T} w_t \mathbb{E}\left[\ell\left(\alpha\sigma^2_{S,t}Z + \alpha_t\sigma^2_{R,t}Z_t\right)\right]. \tag{71}$$

Given the constraint $\alpha s + \sum_{t=1}^{T} \alpha_t(r-s) = \sum_j a_{jj}^2 \le r$, $0 \le \alpha, \alpha_t \le 1$, we complete the proof of Lemma B.1. □

Given this result we can now analyze the generalization error when predicting on the target task $\mathcal{D}_t$.

Lemma B.2. *Consider any $t \in [T]$. Let $v_{t,1} = \sum_{j\in S}(u_t^*)_j^2$ and $v_{t,2} = \sum_{j\in P_t}(u_t^*)_j^2$. Suppose in ϕ^* (calculated in Lemma B.1), $\alpha, \alpha_t > 0$. Suppose the prediction loss ℓ_c is L-Lipschitz.*

Then the Empirical Risk Minimizer $\hat{u}_t \in \mathcal{F}_{\phi^*,t}$ on ϕ^* using m labeled data points from $\mathcal{D}_t$ has risk

$$\mathbb{E}_{(x,y)\sim\mathcal{D}_t}[\ell_c(\hat{u}_t{}^\top\phi^*(x), y)] \le 8\sqrt{\frac{2\ln(4/\delta)}{m}}$$
$$+ 4L\sqrt{\frac{1}{m}\left(\frac{v_{t,1}}{\alpha} + \frac{v_{t,2}}{\alpha_t}\right)}\left(\sqrt{s\alpha\sigma^2_{S,t} + (r-s)\alpha_t\sigma^2_{R,t}} + O\left(\sqrt{\frac{\max\{\alpha\sigma^2_{S,t}, \alpha_t\sigma^2_{R,t}\}^2 r}{s\alpha\sigma^2_{S,t} + (r-s)\alpha_t\sigma^2_{R,t}}}\right)\right).$$

Proof. For any $t \in [T]$, we only need to bound the Rademacher complexity $\mathcal{R}_m(\mathcal{F}_{\phi^*,t})$ of $\mathcal{F}_{\phi^*,t}$; the statement then follows from standard generalization bounds,

$$\mathbb{E}_{(x,y)\sim\mathcal{D}_t}[\ell_c(\hat{u}_t{}^\top\phi^*(x), y)] \le 4L\mathcal{R}_m(\mathcal{F}_{\phi^*,t}) + 8\sqrt{\frac{2\ln(4/\delta)}{m}}.$$

Given the representation ϕ^* in Lemma B.1, to ensure there exists a predictor in $\mathcal{F}_{\phi^*,t}$ matching the ground-truth label, $f(\phi^*(x)) = u_t^\top\phi^*(x) = y = (u_t^*)^\top z_{R_t}$, predictor u_t should satisfy

$$\mathbb{E}_{\mathcal{D}_t}[(\hat{y}-y)^2] = 0 \Leftrightarrow \forall z_{R_t}, \quad u_t{}^\top[QA^*, \mathbf{0}]M^{-1}M[z_{R_t}; \mathbf{0}; z_U] = u_t^{*\top} z_{R_t} \tag{72}$$

$$\Leftrightarrow \forall z_{R_t}, \quad u_t{}^\top QA^*[z_{R_t}; \mathbf{0}] = u_t^{*\top} z_{R_t} \tag{73}$$

$$\overset{(*)}{\Leftrightarrow} A^*_{1:r,1:r}(Q^\top)_{1:r,1:k}u_t = u_t^* \tag{74}$$

$$\Leftrightarrow \forall v \in \mathbb{R}^r, \quad u_t = Q_{1:k,1:r}(A^*_{1:r,1:r})^{-1}u_t^* + Q_{1:k,r+1:k}v. \tag{75}$$

The $(*)$ is from non-zero variance for z_{R_t}. $u_t = Q_{1:k,1:r}(A^*_{1:r,1:r})^{-1}u_t^*$ is the least-norm optimal solution, so we have $B_{\phi^*,t} = \|Q_{1:k,1:r}(A^*_{1:r,1:r})^{-1}u_t^*\| = \sqrt{\frac{v_{t,1}}{\alpha} + \frac{v_{t,2}}{\alpha_t}}$. So the predictor class should be

$$\mathcal{F}_{\phi^*,t} = \left\{f(\phi^*) = u_t^\top\phi^* : u_t \in \mathbb{R}^k, \|u_t\| \le B_{\phi^*,t} = \sqrt{\frac{v_{t,1}}{\alpha} + \frac{v_{t,2}}{\alpha_t}}\right\}. \tag{76}$$

The empirical Rademacher complexity and Rademacher complexity of $\mathcal{F}_{\phi^*,t}$ with m samples are

$$\hat{\mathcal{R}}_m(\mathcal{F}_{\phi^*,t}) = \frac{1}{m}\mathbb{E}_\sigma\left[\sup_{f_{u,\phi}\in\mathcal{F}_{\phi^*,t}} \sum_{i=1}^{m} \sigma_i f_{u,\phi}(x^{(i)})\right] \tag{77}$$

$$= \frac{1}{m}\mathbb{E}_\sigma\left[\sup_{\|u\|\le B_{\phi^*,t}} \sum_{i=1}^{m} \sigma_i u_t{}^\top QA^*[z_{R_t}^{(i)}; \mathbf{0}]\right] \tag{78}$$

$$= \frac{1}{m}\mathbb{E}_\sigma\left[\sup_{\|u\|\le B_{\phi^*,t}} u_t{}^\top \sum_{i=1}^{m} \sigma_i Q_{1:k,1:r}A^*_{1:r,1:r}z_{R_t}^{(i)}\right] \tag{79}$$

$$= \frac{B_{\phi^*,t}}{m}\mathbb{E}_\sigma\left[\left\|\sum_{i=1}^{m} \sigma_i Q_{1:k,1:r}A^*_{1:r,1:r}z_{R_t}^{(i)}\right\|\right], \tag{80}$$

$$\mathcal{R}_m(\mathcal{F}_{\phi^*,t}) = \mathbb{E}_{z_R,z_U}\left[\hat{\mathcal{R}}_m(\mathcal{F}_{\phi^*,t})\right] \tag{81}$$

$$= \frac{B_{\phi^*,t}}{m}\mathbb{E}_{z_{R_t}^{(i)}}\left[\mathbb{E}_\sigma\left[\left\|\sum_{i=1}^m \sigma_i Q_{1:k,1:r} A^*_{1:r,1:r} z_{R_t}^{(i)}\right\|\right]\right] \tag{82}$$

$$= \frac{B_{\phi^*,t}}{m}\mathbb{E}_{z_{R_t}^{(i)}}\left[\left\|A^*_{1:r,1:r}\sum_{i=1}^m z_{R_t}^{(i)}\right\|\right]. \tag{83}$$

For any $t \in [T]$, define $X_t := A^*_{1:r,1:r}\sum_{i=1}^m z_{R_t}^{(i)}$. Note that for $j \in S$, $X_{t,j} = \alpha\sum_{i=1}^m z_j^{(i)}$ is a Gaussian of mean zero and variance $\mathbb{E}[X_{t,j}^2] = \alpha\mathbb{E}\left[\left(\sum_{i=1}^m z_j^{(i)}\right)^2\right] = \alpha\mathbb{E}\left[\sum_{i=1}^m \left(z_j^{(i)}\right)^2\right] = m\alpha\sigma_{S,t}^2$. Similarly, for $j \in P_t$, $X_{t,j} = \alpha_t\sum_{i=1}^m z_j^{(i)}$ is a Gaussian of mean zero and variance $\mathbb{E}[X_{t,j}^2] = m\alpha_t\sigma_{R,t}^2$. Since $X_{t,j}$ is sub-gaussian, $X_{t,j}^2 - m\alpha\sigma_{S,t}^2$ for $j \in S$ and $X_{t,j}^2 - m\alpha_t\sigma_{R,t}^2$ for $j \in P_t$ are sub-exponential and more precisely

$$\|X_{t,j}^2 - m\alpha\sigma_{S,t}^2\|_{\psi_1} \le C_1\|X_{t,j}^2\|_{\psi_1} = C_1\|X_{t,j}\|_{\psi_2}^2 \le C_2 m\alpha\sigma_{S,t}^2, \quad j \in S, \tag{84}$$

$$\|X_{t,j}^2 - m\alpha_t\sigma_{R,t}^2\|_{\psi_1} \le C_1\|X_{t,j}^2\|_{\psi_1} = C_1\|X_{t,j}\|_{\psi_2}^2 \le C_2 m\alpha_t\sigma_{R,t}^2, \quad j \in P_t, \tag{85}$$

where C_1, C_2 are absolute constants and $C_2 > 1$. Let $K = \max(C_2 m\alpha\sigma_{S,t}^2, C_2 m\alpha_t\sigma_{R,t}^2) = C_2 m\max\{\alpha\sigma_{S,t}^2, \alpha_t\sigma_{R,t}^2\}$ and $\mu := m(s\alpha\sigma_{S,t}^2 + (r-s)\alpha_t\sigma_{R,t}^2)$. By Bernstein's inequality, we have for every $\gamma \ge 0$ that

$$\mathbb{P}\left\{\left|\frac{1}{r}(\|X_t\|^2 - \mu)\right| \ge \gamma\right\} \le 2\exp\left[-c\min\left(\frac{\gamma^2}{K^2}, \frac{\gamma}{K}\right)r\right] \tag{86}$$

$$\Rightarrow \mathbb{P}\left\{\left|\frac{\|X_t\|^2}{\mu} - 1\right| \ge \frac{r\gamma}{\mu}\right\} \tag{87}$$

$$\le 2\exp\left[-\frac{c}{C_2^2}\min\left(\frac{\gamma^2}{m^2\max\{\alpha\sigma_{S,t}^2, \alpha_t\sigma_{R,t}^2\}^2}, \frac{\gamma}{m\max\{\alpha\sigma_{S,t}^2, \alpha_t\sigma_{R,t}^2\}}\right)r\right], \tag{88}$$

where c is an absolute constant. For all numbers $z \ge 0$, we have $|z-1| \ge \delta \Rightarrow |z^2 - 1| \ge \max(\delta, \delta^2)$. Thus, for any $\delta \ge 0$, we have

$$\mathbb{P}\left\{\left|\frac{\|X_t\|}{\sqrt{\mu}} - 1\right| \ge \delta\right\} \tag{89}$$

$$\le \mathbb{P}\left\{\left|\frac{\|X_t\|_2^2}{\mu} - 1\right| \ge \max(\delta, \delta^2)\right\} \tag{90}$$

$$\le 2\exp\left[-\frac{c}{C_2^2}\min\left(\left(\frac{\mu\max(\delta,\delta^2)}{m\max\{\alpha\sigma_{S,t}^2, \alpha_t\sigma_{R,t}^2\}r}\right)^2, \frac{\mu\max(\delta,\delta^2)}{m\max\{\alpha\sigma_{S,t}^2, \alpha_t\sigma_{R,t}^2\}r}\right)r\right] \tag{91}$$

$$\le 2\exp\left[-\frac{c}{C_2^2}\left(\frac{\mu}{m\max\{\alpha\sigma_{S,t}^2, \alpha_t\sigma_{R,t}^2\}r}\right)^2\min\left(\left(\max(\delta,\delta^2)\right)^2, \max(\delta,\delta^2)\right)r\right] \tag{92}$$

$$= 2\exp\left[-\frac{c}{C_2^2}\frac{\mu^2}{m^2\max\{\alpha\sigma_{S,t}^2, \alpha_t\sigma_{R,t}^2\}^2 r}\delta^2\right], \tag{93}$$

where the last inequality is from $\mu = m(s\alpha\sigma_{S,t}^2 + (r-s)\alpha_t\sigma_{R,t}^2) \le m\max\{\alpha\sigma_{S,t}^2, \alpha_t\sigma_{R,t}^2\}r$. Changing variables to $\theta = \delta\sqrt{\mu}$, we obtain the desired sub-gaussian tail

$$\mathbb{P}\left\{|\|X_t\| - \sqrt{\mu}| \ge \theta\right\} \le 2\exp\left[-\frac{c}{C_2^2}\frac{\mu}{m^2\max\{\alpha\sigma_{S,t}^2, \alpha_t\sigma_{R,t}^2\}^2 r}\theta^2\right]. \tag{94}$$

By generalization of integral identity, we have

$$|\mathbb{E}\left[\|X_t\| - \sqrt{\mu}\right]| = \left|\int_0^\infty \mathbb{P}\{\|X_t\| - \sqrt{\mu} > \theta\}d\theta - \int_{-\infty}^0 \mathbb{P}\{\|X_t\| - \sqrt{\mu} < \theta\}d\theta\right| \tag{95}$$

$$\leq 2\int_0^\infty \mathbb{P}\{|\|X_t\| - \sqrt{\mu}| > \theta\}d\theta \tag{96}$$

$$\leq 4\int_0^\infty \exp\left[-\frac{c}{C_2^2}\frac{\mu}{m^2\max\{\alpha\sigma_{S,t}^2, \alpha_t\sigma_{R,t}^2\}^2 r}\theta^2\right]d\theta \tag{97}$$

$$\leq C_3\frac{m\max\{\alpha\sigma_{S,t}^2, \alpha_t\sigma_{R,t}^2\}\sqrt{r}}{\sqrt{\mu}}, \tag{98}$$

where C_3 is an absolute constant. Thus, we have

$$\left|\mathcal{R}_m(\mathcal{F}_{\phi^*,t}) - \sqrt{\frac{1}{m}\left(\frac{v_{t,1}}{\alpha} + \frac{v_{t,2}}{\alpha_t}\right)(s\alpha\sigma_{S,t}^2 + (r-s)\alpha_t\sigma_{R,t}^2)}\right| \tag{99}$$

$$= \frac{B_{\phi^*,t}}{m}\left|\mathbb{E}\left[\|X_t\| - \sqrt{\mu}\right]\right| \tag{100}$$

$$\leq O\left(\sqrt{\frac{1}{m}\left(\frac{v_{t,1}}{\alpha} + \frac{v_{t,2}}{\alpha_t}\right)\frac{\max\{\alpha\sigma_{S,t}^2, \alpha_t\sigma_{R,t}^2\}^2 r}{s\alpha\sigma_{S,t}^2 + (r-s)\alpha_t\sigma_{R,t}^2}}\right). \tag{101}$$

□

B.2 Proofs of Proposition 2.3 and Proposition 2.4

Given the lemmas for the general case, we are now ready to prove the results in Proposition 2.3 and Proposition 2.4.

Proposition B.3 (Restatement of Proposition 2.3)**.** *Suppose $\sigma_{S,t} = \sigma_{R,t} = \sigma_{U,t} = 1$ for any $t \in [T]$. The representation ϕ^* obtained on an even mixture of data from all the tasks $\{\mathcal{D}_t : 1 \leq t \leq T\}$ satisfies $\phi^* \circ g(z) = Q\left(\sum_{j\in S}\sqrt{\alpha}z_j e_j + \sum_{j\in R\setminus S}\sqrt{\beta}z_j e_j\right)$ for some $\alpha \in [0,1]$, $\beta = \min\left(1, \frac{r-\alpha s}{T(r-s)}\right)$, where e_j's are the basis vectors and Q is any orthonormal matrix.*
The Empirical Risk Minimizer $\hat{u} \in \mathcal{F}_{\phi^*,t}$ on ϕ^* using m labeled data points from $\mathcal{D}_t$ has risk

$$\mathbb{E}_{(x,y)\sim\mathcal{D}_t}[\ell_c(\hat{u}^\top\phi^*(x), y)]$$
$$\leq 4L\sqrt{\frac{1}{m}\left(\frac{v_{t,1}}{\alpha} + \frac{v_{t,2}}{\beta}\right)}\left(\sqrt{s\alpha + (r-s)\beta} + O\left(\sqrt{\frac{r}{s\alpha + (r-s)\beta}}\right)\right) + 8\sqrt{\frac{2\ln(4/\delta)}{m}}.$$

Proof. This follows from Lemma B.1, and considering the optimal α, α_t for the following:

$$g(\{\alpha, \alpha_t\}) = \sum_{t=1}^T w_t\mathbb{E}\left[\ell\left(\alpha\sigma_{S,t}^2 Z + \alpha_t\sigma_{R,t}^2 Z_t\right)\right] \tag{102}$$

$$= \frac{1}{T}\sum_{t=1}^T \mathbb{E}\left[\ell\left(\alpha Z + \alpha_t Z_1\right)\right] \tag{103}$$

$$\geq \mathbb{E}\left[\ell\left(\alpha Z + Z_1\sum_{t=1}^T\frac{1}{T}\alpha_t\right)\right]. \tag{104}$$

The second equation is from that Z_t's follow the same distribution by the symmetry of $\tilde{z}_j$'s. The inequality comes from the convexity of $\ell(t)$ and Jensen's inequality. So the minimum is achieved when $\alpha_t := \beta$ for any $t \in [T]$, leading to

$$g(\{\alpha, \alpha_t\}) = \mathbb{E}\left[\ell\left(\alpha Z + \beta Z_1\right)\right] \tag{105}$$

subject to the constraints $\alpha s + T\beta(r-s) \le r$, $0 \le \alpha, \beta \le 1$. Then we get $\phi^* \circ g(z) = W^* M z = Q\left(\sum_{j\in S}\sqrt{\alpha} z_j e_j + \sum_{j\in R\setminus S}\sqrt{\beta} z_j e_j\right)$ for some $\alpha \in [0,1],\ \beta = \min\left(1, \frac{r-\alpha s}{T(r-s)}\right)$, where e_j's are the basis vectors and Q is any orthonormal matrix.

Finally, the generalization bound follows from Lemma B.2, and that

$$O\left(\sqrt{\frac{\max\{\alpha,\beta\}^2 r}{s\alpha + (r-s)\beta}}\right) = O\left(\sqrt{\frac{r}{s\alpha + (r-s)\beta}}\right). \tag{106}$$

This completes the proof. □

Proposition B.4 (Restatement of Proposition 2.4)**.** *Suppose $\sigma_{S,t} = \sigma_{R,t} = \sigma_{U,t} = 1$. The representation ϕ_t^* obtained on data from $\mathcal{D}_t$ satisfies $\phi_t^* \circ g(z) = Q\left(\sum_{j\in R_t} z_j e_j\right)$ where e_j's are the basis vectors and Q is any orthonormal matrix.*
The Empirical Risk Minimizer $\hat{u} \in \mathcal{F}_{\phi_t^*,t}$ on ϕ_t^* using m labeled data points from $\mathcal{D}_t$ has risk

$$\mathbb{E}_{(x,y)\sim\mathcal{D}_t}[\ell_c(\hat{u}^\top \phi_t^*(x), y)] \le 4L\sqrt{\frac{r}{m}}\|u_t^*\| + 8\sqrt{\frac{2\ln(4/\delta)}{m}}.$$

While on task $\mathcal{D}_i (i \ne t)$, any linear predictor on ϕ_t^* has error at least $\min_u \mathbb{E}_{\mathcal{D}_i}[\ell_c(u^\top z_S, y)]$.

Proof. Following Lemma B.1 (with $r = s$), we get $\phi_t^* \circ g(z) = Q\left(\sum_{j\in R_t} z_j e_j\right)$, where e_j's are the basis vectors and Q is any orthonormal matrix. Following the same argument as in the proof of Lemma B.2, we get

$$\mathcal{R}_m(\mathcal{F}_{\phi^*,t}) = \frac{\|u_t^*\|}{m}\mathbb{E}_{z_{R_t}^{(i)}}\left[\left\|\sum_{i=1}^m z_{R_t}^{(i)}\right\|\right] \tag{107}$$

$$\le \sqrt{\frac{r}{m}}\|u_t^*\|, \tag{108}$$

where the last inequality comes from the property of chi-squared distribution expectation. □

B.3 Implication for the trade-off

The propositions then imply the trade-off between universality and label efficiency. Below we formalize the example discussed in Section 2.2.

Proposition B.5 (A specific version of Proposition 2.3)**.** *Suppose $\sigma_{S,t} = \sigma_{R,t} = \sigma_{U,t} = 1$ for any $t \in [T]$ and $r = 2s$. The representation ϕ^* obtained on an even mixture of data from all the tasks $\{\mathcal{D}_t : 1 \le t \le T\}$ satisfies $\phi^* \circ g(z) = Q\left(\sum_{j\in S} z_j e_j + \sum_{j\in R\setminus S}\sqrt{\frac{1}{T}} z_j e_j\right)$, where e_j's are the basis vectors and Q is any orthonormal matrix.*
The Empirical Risk Minimizer $\hat{u} \in \mathcal{F}_{\phi^*,t}$ on ϕ^* using m labeled data points from $\mathcal{D}_t$ has risk

$$\mathbb{E}_{(x,y)\sim\mathcal{D}_t}[\ell_c(\hat{u}^\top \phi^*(x), y)] \le \quad 4L\sqrt{\frac{1}{m}\left(v_{t,1} + Tv_{t,2}\right)}\left(\sqrt{r\left(\frac{T+1}{2T}\right)} + O(1)\right) + 8\sqrt{\frac{2\ln(4/\delta)}{m}}.$$

Proof. This follows from Proposition 2.3, and noting that when $r = 2s$, $\alpha = 1$ and $\beta = 1/T$ are the optimal for:

$$g(\{\alpha,\beta\}) = \mathbb{E}\left[\ell\left(\alpha Z + \beta Z_1\right)\right] \tag{109}$$

$$= \mathbb{E}\left[\ell\left(\alpha Z + \frac{r-\alpha s}{T(r-s)} Z_1\right)\right] \tag{110}$$

$$= \mathbb{E}\left[\ell\left(\alpha Z + \frac{2-\alpha}{T} Z_1\right)\right] \tag{111}$$

subject to the constraints $\alpha s + T\beta(r-s) \le r$, $0 \le \alpha, \beta \le 1$. To see this, note that $Z \sim \chi_s^2$ and $Z_1 \sim \chi_{r-s}^2 = \chi_s^2$ follow the same distribution, so $\alpha Z + \frac{2-\alpha}{T} Z_1$ for $\alpha = 1$ will stochastically dominate its value for other $\alpha \in [0,1)$. The optimal is then achieved when $\alpha = 1$ and $\beta = \frac{2-\alpha}{T} = \frac{1}{T}$. □

B.4 IMPROVING THE TRADE-OFF BY CONTRASTIVE REGULARIZATION

The above analysis shows that contrastive learning a representation on unlabeled data from the target task can help prediction on this target task. This suggests that given a representation ϕ^* pre-trained on diverse data, one can fine-tune it by contrastive learning on some unlabeled data from the target task to get a representation that can lead to better prediction on the target task. In the following, we will formally show that this is indeed the case for the illustrative example in Section 2.2.

Recall that in this example, $\sigma_{S,t} = \sigma_{R,t} = \sigma_{U,t} = 1$, $r = 2s$, and $v_{t,1} = v_{t,2}$. The representation ϕ^* obtained on an even mixture of data from all the tasks $\{\mathcal{D}_t : 1 \leq t \leq T\}$ satisfies $\phi^* \circ g(z) = Q\left(\sum_{j\in S}\sqrt{\alpha}z_je_j + \sum_{j\in R\setminus S}\sqrt{\beta}z_je_j\right)$, where e_j's are the basis vectors and Q is any orthonormal matrix, and $\alpha = 1, \beta = \frac{1}{T}$.

Now, suppose we are given unlabeled data from $\mathcal{D}_t$, and we use them to fine-tune $\phi^*(x) = W^*x$ by contrastive learning on these unlabeled data. That is, we find W near W^* to minimize the contrastive loss on the unlabeled data from $\mathcal{D}_t$:

$$\min_{\phi(x)=Wx} \mathbb{E}\left[\ell\left(\phi(x)^\top(\phi(x^+) - \mathbb{E}_{x^-}\phi(x^-))\right)\right] \tag{112}$$

$$\text{subject to} \quad \|W - W^*\|_F \leq \gamma, \|W\| \leq 1. \tag{113}$$

for some small $\gamma > 0$.

Proposition B.6. *For (112), $\phi^*_{CR,t}$ satisfying the following on x from $\mathcal{D}_t$ is an optimal representation:*

$$\phi^*_{CR,t} \circ g(z) = Q\left(\sum_{j\in S}\sqrt{\alpha}z_je_j + \sum_{j\in P_t}\sqrt{\beta}z_je_j\right)$$

where $\sqrt{\alpha} = 1, \sqrt{\beta} = \min\left(1, \sqrt{\frac{1}{T}} + \frac{\gamma}{\sqrt{s}}\right)$.

Proof. Following the argument in Lemma B.1, we still have that $\phi^*_{\text{CR,t}}(x) = Wx$ where $W = Q_2[A_2; \mathbf{0}]M^{-1}$ for any orthonormal matrix Q_2 and some diagonal matrix $A_2 = \text{diagonal}(a_{jj})$, with $a_{jj} = \sqrt{\alpha}$ for $j \in S$ and $a_{jj} = \sqrt{\beta}$ for $j \in P_t$ for some $\alpha, \beta \in [0, 1]$. And the contrastive loss is:

$$\mathbb{E}\left[\ell\left(\phi(x)^\top(\phi(x^+) - \mathbb{E}_{x^-}\phi(x^-))\right)\right] = \mathbb{E}\left[\ell\left(\sum_{j\in R_t} a_{jj}^2 z_j^2\right)\right] \tag{114}$$

$$= \mathbb{E}\left[\ell\left(\alpha\sum_{j\in S} z_j^2 + \beta\sum_{j\in P_t} z_j^2\right)\right]. \tag{115}$$

Recall that $\phi^*(x) = W^*x$ with $W = Q[A; \mathbf{0}]M^{-1}$ for any orthonormal matrix Q and some diagonal matrix A, with $A_{jj} = 1$ for $j \in S$ and $A_{jj} = \sqrt{1/T}$ for $j \in R_i \setminus S$ for any $i \in [T]$. Then

$$\|W - W^*\|_F = \|Q_2[A_2; \mathbf{0}]M^{-1} - Q[A; \mathbf{0}]M^{-1}\|_F \tag{116}$$

$$= \|Q_2A_2 - QA\|_F \tag{117}$$

$$= \|A_2 - Q_2^{-1}QA\|_F. \tag{118}$$

Since $Q_2^{-1}Q$ is a rotation and A, A_2 are diagonal, we can always set $Q_2 = Q$ without increasing $\|W - W^*\|_F$. Then

$$\|W - W^*\|_F^2 = \|A_2 - A\|_F^2 \tag{119}$$

$$= s(\sqrt{\alpha} - 1)^2 + s(\sqrt{\beta} - \sqrt{1/T})^2 + \sum_{j\in P_i, i\neq t}((A_2)_{jj} - \sqrt{1/T})^2. \tag{120}$$

To minimize the contrastive loss, we need α, β to be as large as possible, subject to $\|W - W^*\|_F^2 \leq \gamma^2$, and $\alpha, \beta, (A_2)_{jj}^2 \in [0, 1]$. The optimal is then achieved when $\alpha = 1, \sqrt{\beta} = \min\left(1, \sqrt{\frac{1}{T}} + \frac{\gamma}{\sqrt{s}}\right)$, and $(A_2)_{jj} = \sqrt{1/T}$ for $j \in P_i, i \neq t$. □

Now, recall that by Proposition 2.3, the ERM has risk:

$$
\begin{aligned}
&\mathbb{E}_{(x,y)\sim\mathcal{D}_t}[\ell_c(\hat{u}^\top \phi^*(x), y)] \\
&\leq 4L\sqrt{\frac{1}{m}\left(\frac{v_{t,1}}{\alpha}+\frac{v_{t,2}}{\beta}\right)}\left(\sqrt{s\alpha+(r-s)\beta}+O\left(\sqrt{\frac{r}{s\alpha+(r-s)\beta}}\right)\right)+8\sqrt{\frac{2\ln(4/\delta)}{m}} \\
&= 4L\sqrt{\frac{1}{m}\left(\frac{\|u_t^2\|^2}{2\alpha}+\frac{\|u_t^2\|^2}{2\beta}\right)}\left(\sqrt{s\alpha+s\beta}+O\left(1\right)\right)+8\sqrt{\frac{2\ln(4/\delta)}{m}} \\
&= O\left(L\sqrt{\frac{r\|u_t^*\|^2}{m}\left(2+\frac{\alpha}{\beta}+\frac{\beta}{\alpha}\right)}\right)
\end{aligned}
$$

With the fine-tuning using contrastive learning, in the representation learned, α remains to be 1, while β increases from $1/T$ to $(\sqrt{1/T}+\gamma/\sqrt{s})^2$. Then the error bound decreases. This shows that the fine-tuning with contrastive learning on unlabeled data from the target task can emphasize the task-specific features z_{P_t}, which then leads to better prediction performance.

C More Experiments Details and Results

C.1 Dataset

CIFAR-10. CIFAR-10 (Krizhevsky et al., 2009) dataset consists of 60,000 32×32 color images in 10 classes: airplane, automobile, bird, cat, deer, dog, frog, horse, ship, truck. Each class has 6,000 images. There are 50,000 training images and 10,000 test images.

CINIC-10. CINIC-10 (Darlow et al., 2018) consists of 32×32 color images from both CIFAR and ImageNet and has 90,000 training images with ten classes identical to CIFAR-10.

SVHN. The Street View House Numbers (Netzer et al., 2011) contains 10 digits color images of size 32×32 in the natural scene. It has 73,257 digits for training and 26,032 digits for testing.

GTSRB. The German Traffic Sign Recognition Benchmark (Stallkamp et al., 2012) is a dataset of color images depicting 43 different traffic signs. The images are not of fixed dimensions and have a rich background and varying light conditions as expected of photographed images of traffic signs. The original training set contains 34,799 images, and the original test set contains 12,630 images. We resize each image to 32×32. The dataset has a significant imbalance in the number of sample occurrences across classes. We use data augmentation techniques to enlarge the training data and balance the number of samples in each class. We construct a class preserving data augmentation pipeline consisting of rotation, translation, and projection transforms and apply this pipeline to the training images until each class contains 2,500 examples. So we construct a new training set containing 107,500 images in total. We also construct a new test set by randomly selecting 10,000 images from the original test set for evaluation.

ImageNet. ImageNet (Deng et al., 2009) is a huge visual dataset which is composed of 1,281,167 training data and 50,000 test data with 1,000 labels. We crop each color image to 224×224 as the standard setting.

ImageNet32. ImageNet32 (Deng et al., 2009) is a huge dataset made up of small color images called the down-sampled version of ImageNet. ImageNet32 is composed of 1,281,167 training data and 50,000 test data with 1,000 labels. Each color image is down-sampled to 32×32.

MNIST. The Modified National Institute of Standards and Technology (LeCun et al., 1998) is a database of handwritten gray-scale digits of size 28×28. It contains 60,000 training images and 10,000 testing images.

EMNIST. Extended MNIST (Cohen et al., 2017) includes gray images of handwritten letters and digits. The images in EMNIST were converted into the same size 28×28 by the same process as MNIST. EMNIST-Letters has 145,600 lower case characters with 26 balanced classes, and EMNIST-Digits has 280,000 characters with ten balanced classes.

Fashion-MNIST. Fashion-MNIST (Xiao et al., 2017) is a dataset of 28×28 gray-scale images with ten classes: T-shirt/top, trouser, pullover, dress, coat, sandal, shirt, sneaker, bag, ankle boot. The training set size is 60,000, and the test set size is 10,000.

Fer2013. Fer2013 is a dataset (Goodfellow et al., 2013) of 48×48 gray-scale images with 7 face expression classes: angry, disgust, fear, happy, sad, surprise, neutral. The training set size is 28,709, and the test set size is 3,589.

FaceScrub. FaceScrub (Ng & Winkler, 2014) is a dataset with 141,130 color face images of 695 public figures.

IMDB. IMDB (Maas et al., 2011) is a large movie review text dataset. The dataset is for binary sentiment classification, positive review or negative review. The dataset contains 25,000 movie reviews for training and 25,000 for testing.

AGNews. AGNews (Zhang et al., 2015) is a sub-dataset of AG's corpus of news articles for text topic classification. It covers the 4 largest classes: world, sports, business, sci/tech. The AG News contains 30,000 training and 1,900 test samples per class.

C.2 Verifying the Existence of the Trade-off

Model. We evaluate three popular contrastive learning frameworks, MoCo v2 (He et al., 2020), NNCLR (Dwibedi et al., 2021) and SimSiam (Chen & He, 2021) . MoCo v2 can be regarded as SimCLR (Chen et al., 2020) equipped with a memory bank, while NNCLR uses nearest-neighbor as the positive pairs. SimSiam can be regarded as a modification from BYOL (Grill et al., 2020) similar to Barlow Twins (Zbontar et al., 2021), which does not need negative pairs. We follow the same data augmentation methods as SimSiam (Chen & He, 2021) for all datasets.

Datasets. We consider three sets of data. In the first set, our downstream task is CIFAR-10, and the pre-training datasets may include CINIC-10, SVHN, GTSRB, and ImageNet32. CINIC-10 has classes identical to CIFAR-10 and is the most target-relevant, while the others are less similar to CIFAR-10. This then provides more and more diverse pre-training data w.r.t. the target task. In the second set, our downstream task is MNIST, and the pre-training datasets may include EMNIST-Digits&Letters, Fashion-MNIST, GTSRB, and ImageNet32. Here, the handwritten dataset EMNIST-Digits&Letters is the most target-relevant. In the last set, our downstream task is Fer2013, a face expression classification dataset. The pre-training datasets may include FaceScrub, CIFAR-10, SVHN, and ImageNet32, where the face dataset Facescrub is the most target-relevant.

Evaluation & Methods. We pre-train a ResNet18 network (He et al., 2016) as a feature extractor under different contrastive learning method using SGD for 800 epochs with a cosine learning-rate scheduler, base learning rate of 0.06, weight decay 5e-4, momentum 0.9 and batch size 512. Then we fix the pre-trained feature extractor, and train a linear classifier (Linear Probing, LP) on $1\%, 5\%, 10\%, 20\%, 100\%$ of the labeled data from the downstream task. For LP we use SGD for 200 epochs with a cosine learning-rate scheduler, base learning rate of 5.0, no weight decay, momentum 0.9 and batch size 256. We finally report the test accuracy on a specific target task and the weighted average test accuracy on all pre-training datasets (i.e., using them as the downstream tasks). We use the class number of each pre-training dataset as the weight, which is consistent with random guessing as a baseline. We have three types of models pre-trained on three sets of datasets. Thus, we have nine tasks in total. For each task, we have two pre-trained models initialized by different random seeds. We evaluated each model three times and we report the average test accuracy with standard deviation based on multiple runs (six evaluations).

In Figs. 7(a)(b)(c), we report results for MoCo v2, NNCLR, SimSiam (respectively) on CIFAR-10 as the downstream task. The size and diversity of unlabeled data for pre-training are increased on the x-axis by incrementally adding datasets in the following order: CINIC-10 (C), SVHN (S), GTSRB (G), and ImageNet32 (only use a 500k subset) (I). Then, we do LP on CIFAR-10 using different proportions of labeled samples. Similarly, in Figs. 7(d)(e)(f), we report results for three models on MNIST. We incrementally add pretraining datasets in the following order: EMNIST-Digits&Letters (E), Fashion-MNIST (F), GTSRB (G), ImageNet32 (I). In Figs. 7(g)(h)(i), the downstream task is Fer2013 and we incrementally add datasets in the following order: FaceScrub (I), CIFAR-10 (C), SVHN (S), ImageNet32 (I).

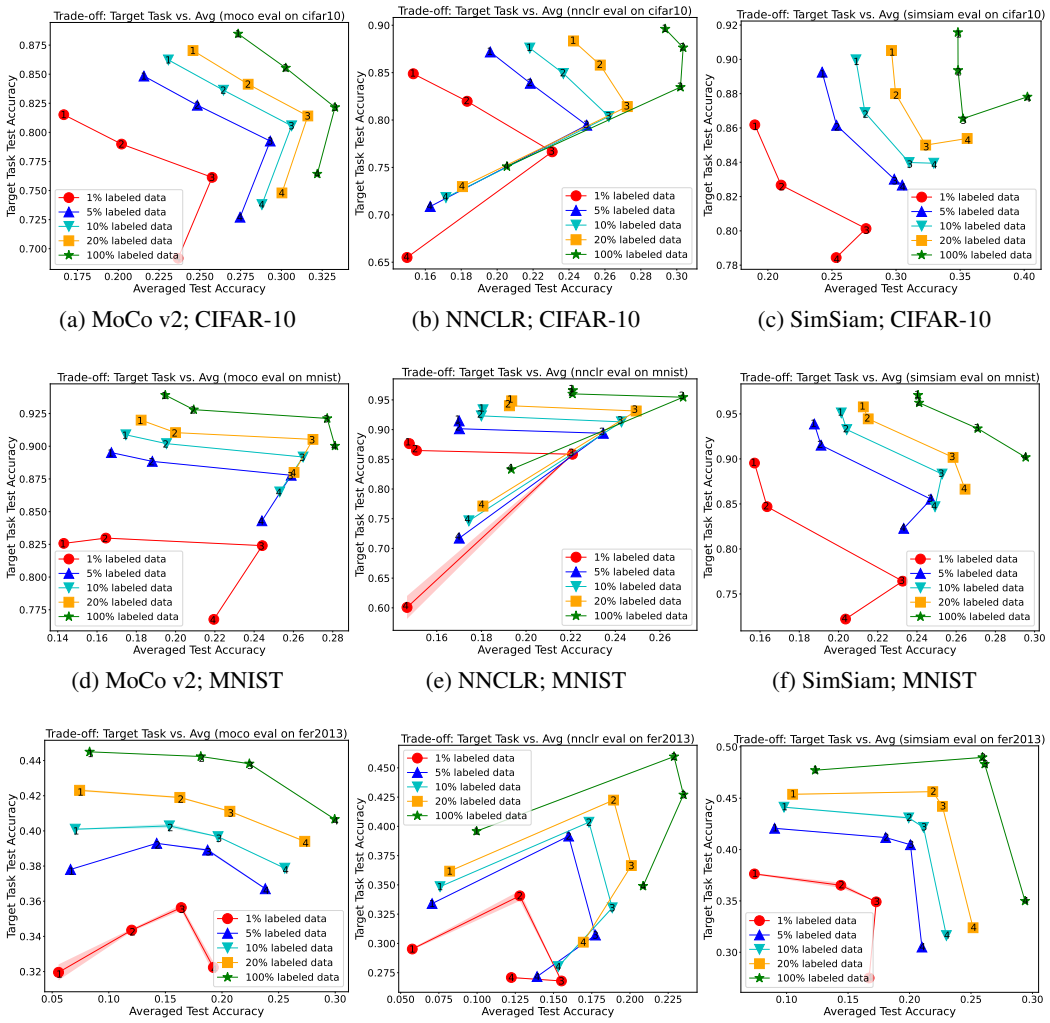

(a) MoCo v2; CIFAR-10 (b) NNCLR; CIFAR-10 (c) SimSiam; CIFAR-10

(d) MoCo v2; MNIST (e) NNCLR; MNIST (f) SimSiam; MNIST

(g) MoCo v2; Fer2013 (h) NNCLR; Fer2013 (i) SimSiam; Fer2013

Figure 7: Trade-off of universality and label efficiency for MoCo v2, NNCLR, SimSiam on downstream tasks CIFAR-10, MNIST, Fer2013. "1, 2, 3, 4" means incrementally adding datasets for pre-training. The x-axis is the average test accuracy of Linear Probing on all 4 datasets. The y-axis is test accuracy on the target task. Pre-training data: (a)(b)(c) CINIC-10, SVHN, GTSRB, and ImageNet32. Target task: CIFAR-10. (d)(e)(f) EMNIST-Digits&Letters, Fashon-MNIST, GTSRB, ImageNet32. Target: MNIST. (g)(h)(i) FaceScrub, CIFAR-10, SVHN, ImageNet32. Target: Fer2013.

Results. In Figs. 7, when the pre-training data becomes more diverse, the average test accuracy on all pre-training datasets increases (i.e., universality improves), while the test accuracy on the specific target task decreases (i.e., label efficiency drops). This shows a clear trade-off between universality and label efficiency. Moreover, with fewer labeled data (from green line to red line), the trade-off phenomenon will be more significant. It supports our claim that diverse pre-training data allow learning diverse features for better universality, but can down-weight the features for a specific task resulting in worse prediction. As more diverse unlabeled data are included, more labeled data from the target task is needed to achieve comparably-good prediction accuracy. This validates our analysis about the trade-off in Section 2.2.

In Figs. 7(a)(b)(d)(e)(f)(h), the average test accuracy (x-axis) decreases in the end because when we add one pre-training dataset, it may hurt the test accuracy of all other pre-training datasets. In

Figs. 7(g)(h), the downstream task test accuracy (y-axis) increases in the beginning because when the pre-training unlabeled data from relevant tasks is not sufficiently large, introducing other pre-training datasets will help the model to learn features relevant for the downstream task. However, the downstream task test accuracy will drop later as in other figures.

Please refer to Appendix C.5 for more figures.

C.3 INSPECTING THE TRADE-OFF

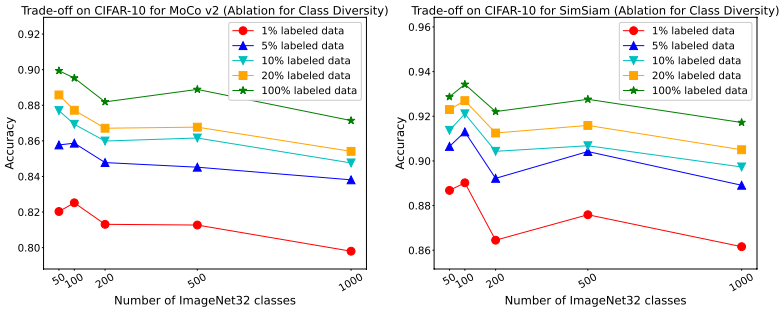

(a) MoCo v2 (b) SimSiam

Figure 8: Pre-train MoCo v2 and SimSiam on CIFAR-10 + ImageNet32(200k) with varying number of classes of ImageNet32 from 50 to 1000 (x-axis) under a fixed size of pre-training data. The y-axis is LP test accuracy on CIFAR-10.

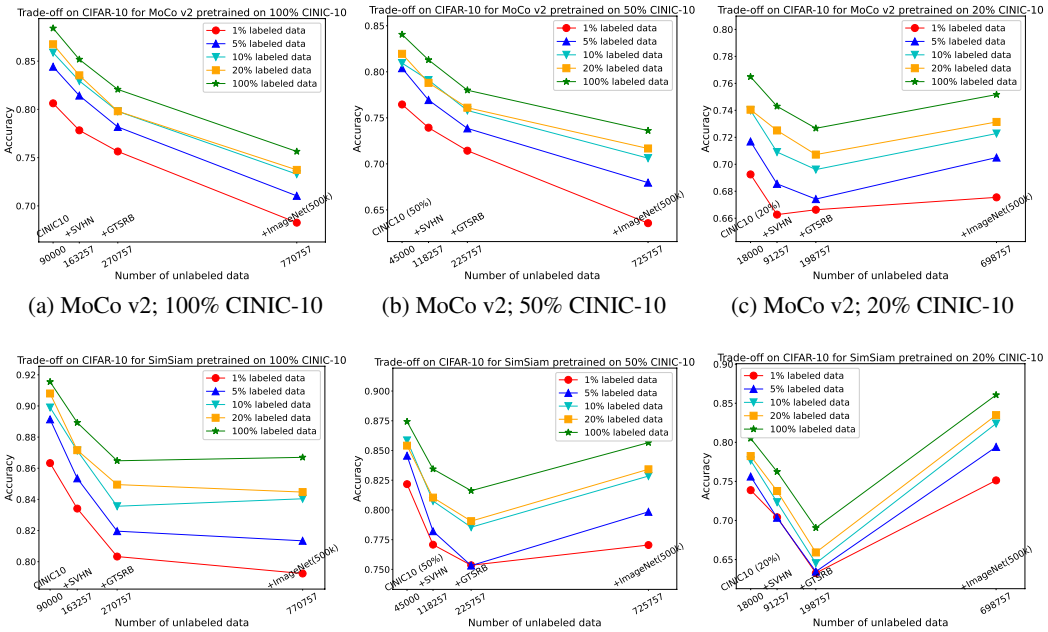

(a) MoCo v2; 100% CINIC-10 (b) MoCo v2; 50% CINIC-10 (c) MoCo v2; 20% CINIC-10

(d) SimSiam; 100% CINIC-10 (e) SimSiam; 50% CINIC-10 (f) SimSiam; 20% CINIC-10

Figure 9: Trade-off on CIFAR-10 LP test accuracy (y-axis) for MoCo v2 and SimSiam with varying target relevant (CINIC-10) pre-training data percentage (100%, 50%, 20%).

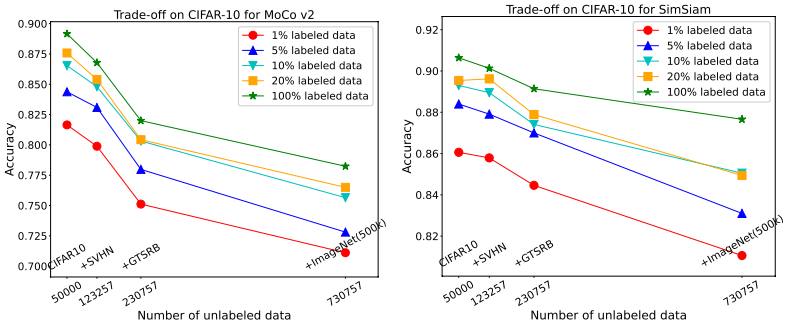

Figure 10: Trade-off on CIFAR-10 LP test accuracy (y-axis) for MoCo v2 and SimSiam pre-trianed on datasets including CIFAR-10.

C.3.1 Ablation Study

We report results from three ablation studies: (1) varying the class number of ImageNet32, (2) varying the percentage of target-relevant pre-training data, and (3) replacing CINIC-10 with CIFAR-10 in the pre-training dataset.

Varying the Class Number of ImageNet32. To further support **A1**, we show that the trade-off between universality and label efficiency also exists under a fixed dataset size. In Fig. 8, we pre-train MoCo v2 and SimSiam on CIFAR-10 + ImageNet32(200k) and keep the same setting as Fig. 7 except that we vary the class number of ImageNet32(200k). In previous experiments, we randomly pick 500,000 images from ImageNet32 without considering labels. Here, we fix the number of classes to 50, 100, 200, 500, 1000. Then we randomly sample 200,000 images from the subset of classes. The downstream task is CIFAR-10. In Fig. 8, we observe that with a fixed pre-training datasets size, e.g., 250,000, when the data is more diverse, the pre-training will learn more irrelevant features, and the performance will drop on the downstream task. This supports our analysis as well.

Varying Target-Relevant pre-training Data Percentage. In Fig. 9, we use (a)(d) 100% (b)(e) 50% (c)(f) 20% CINIC-10 to train MoCo v2 and SimSiam, and keep the same setting as Fig. 7. For Fig. 9 (b) with 50% CINIC-10, test accuracy drops, e.g., the test accuracy of 1% CIFAR-10 in Fig. 9 (a) 80.63% vs. (b) 76.45%. We can also see the decreasing curve in Fig. 9 (b). On the other hand, we also have test accuracy drops in Fig. 9 (c) (e) (f). However, we can see a U-curve rather than a strictly decreasing curve in Fig. 9 (c) (e) (f). ImageNet32 is more relevant with CIFAR-10 than SVHN and GTSRB, consistent with human intuition. When we have a small partition of CINIC-10 which does not cover all target relevant features, the feature extractor can learn these missing features from ImageNet32. Although there are many irrelevant features in ImageNet32, the positive effect is larger than the negative effect, and so it plots a U-curve. It is consistent with our statement that we need a large and target relevant pre-training dataset rather than a diverse irrelevant one.

Replacing CINIC-10 With CIFAR-10. In Fig. 10, we keep the same setting as Fig. 7 except we replace CINIC-10 with CIFAR-10. Note that our downstream task is still CIFAR-10. In Fig. 10, we can see the same phenomena and similar performance as Fig. 7. Thus, if we have a good choice of a task-relevant pre-training dataset, we can get similar performance as pre-training on the downstream task domain directly.

The pre-training unlabeled data from diverse tasks may have a positive effect when the pre-training unlabeled data from similar (relevant) tasks is not sufficiently large. Moreover, if we choose a good task-relevant pre-training dataset, we can directly get similar performance as pre-training on the downstream task. However, when the task-relevant dataset is sufficient, the performance will drop if we introduce task-irrelevant data in the pre-training dataset (Fig. 9 (a)(d)).

C.3.2 Feature Similarity

For each set of pre-training data, we extract a set of features for the target task, CIFAR-10, MNIST and Fer2013 respectively, using the pre-trained representation function. In Fig. 11 (rows/columns are pre-training data; numbers/colors show the similarity) first row, the features from different pre-

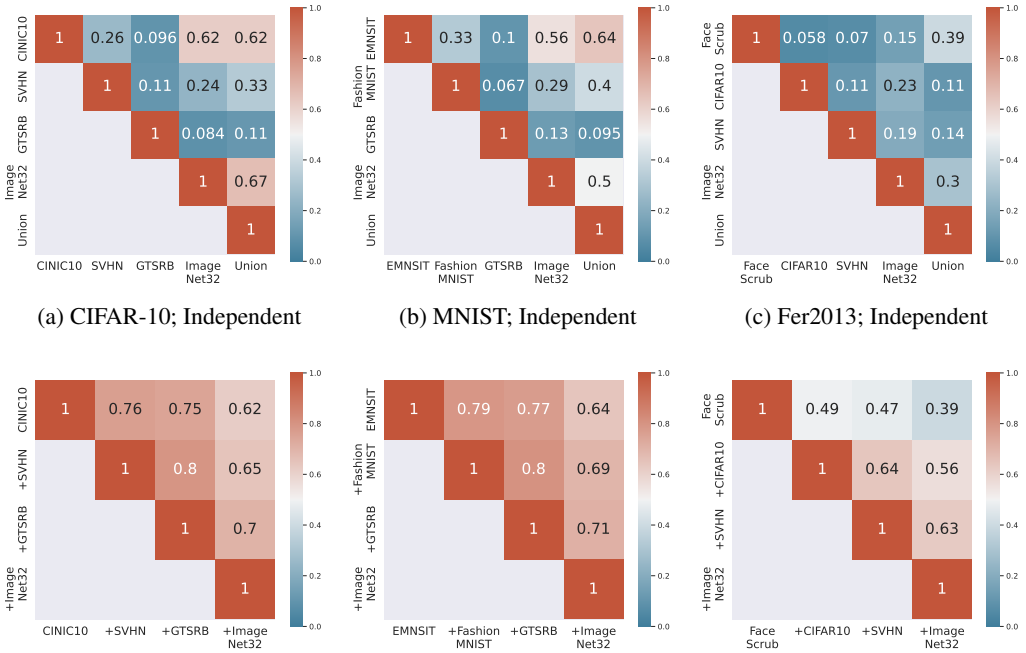

(a) CIFAR-10; Independent (b) MNIST; Independent (c) Fer2013; Independent

(d) CIFAR-10; Incremental (e) MNIST; Incremental (f) Fer2013; Incremental

Figure 11: Linear CKA similarity score among downstream task features from MoCo v2 pre-trained on three sets of datasets. For "Independent", each representation model in the first four columns/rows is pre-trained on a single dataset. "Union" indicates the model pre-trained on the union among four disjoint datasets. "Incremental" means from left column to right, from top row to bottom, we incrementally add datasets for pre-training.

Pretrain data	Method	1% label data	5% label data	10% label data	20% label data	100% label data
CINIC10	LP	80.63±0.01	**84.42±0.01**	85.88±0.05	86.75±0.01	88.41±0.01
	FT	68.74±0.46	81.46±0.34	85.20±0.14	88.69±0.29	93.58±0.14
	Ours	**83.66±0.43**	83.04±0.08	**86.18±0.24**	**89.61±0.12**	**94.51±0.02**
+SVHN	LP	77.83±0.01	81.43±0.04	82.95±0.01	83.53±0.01	85.18±0.01
	FT	66.01±0.52	80.20±0.07	83.96±0.46	88.01±0.07	93.35±0.10
	Ours	**79.95±0.36**	**81.77±0.11**	**84.98±0.02**	**88.97±0.14**	**94.26±0.01**
+GTSRB	LP	75.64±0.01	78.18±0.01	79.80±0.02	79.81±0.01	82.07±0.01
	FT	62.79±0.57	78.90±0.41	83.89±0.03	87.85±0.03	93.42±0.13
	Ours	**76.20±0.36**	**80.26±0.05**	**84.11±0.06**	**88.74±0.01**	**94.32±0.13**
+ImageNet32	LP	68.26±0.01	71.04±0.01	73.29±0.02	73.73±0.02	75.64±0.03
	FT	65.40±0.16	**78.99±0.21**	82.96±0.17	86.75±0.10	92.92±0.06
	Ours	**71.70±1.20**	78.94±0.06	**83.48±0.02**	**87.77±0.13**	**93.66±0.12**

Table 3: Test accuracy on CIFAR-10 with different evaluation methods on MoCo v2 under different percentages of labeled data. From top to bottom: incrementally add datasets for pre-training.

training datasets have low similarities. This is consistent with our setup in Section 2.2 that different tasks only share some features and each owns many private ones. In the second row, we can see a decreasing trend of similarity in each row of each sub-figure. This indicates when gradually adding more diverse pre-training data, the obtained representation will encode more downstream task-irrelevant information and become less similar to that before adding more pre-training data. It will hurt the downstream task performance. This result is consistent with our Proposition 2.3 and 2.4.

Target data	Method	Aug	1% label data	5% label data	10% label data	20% label data	100% label data
ImageNet	LP	1	66.04±0.26	76.28±0.05	78.06±0.02	78.73±0.03	77.84±0.02
	FT	1	71.09±0.05	75.32±0.11	76.38±0.01	76.92±0.10	82.97±0.02
	FT	10	73.28±0.01	76.43±0.14	78.69±0.04	81.56±0.10	83.65±0.01
	FT	100	71.83±0.05	77.55±0.07	80.16±0.09	82.23±0.01	83.58±0.05
	Ours	10	**74.36±0.09**	**78.60±0.03**	80.02±0.08	81.28±0.07	84.94±0.09
	Ours	100	73.03±0.04	78.41±0.04	**80.48±0.05**	**82.42±0.03**	**85.34±0.07**
SVHN	LP	1	59.24±0.02	57.25±0.08	56.32±0.17	58.35±0.08	63.44±0.01
	FT	1	55.20±0.16	61.73±0.32	64.91±0.12	64.70±0.64	65.76±0.10
	FT	10	61.24±0.08	65.89±0.54	68.61±0.52	70.89±0.07	78.22±0.18
	FT	100	65.23±0.03	72.34±0.07	75.13±0.11	77.20±0.03	80.13±0.14
	Ours	10	62.87±0.42	67.56±0.23	70.16±0.02	72.23±0.09	78.72±0.37
	Ours	100	**65.30±0.43**	**72.61±0.07**	**75.34±0.12**	**77.64±0.05**	**82.50±0.01**
GTSRB	LP	1	71.20±0.61	83.97±0.08	85.31±0.02	86.34±0.06	86.56±0.01
	FT	1	77.18±0.40	87.65±0.18	88.56±0.75	88.76±0.01	89.83±0.39
	FT	10	84.55±0.30	88.74±0.32	89.11±0.11	89.52±0.12	90.74±0.06
	FT	100	86.28±0.26	90.50±0.29	90.83±0.08	91.15±0.01	91.89±0.12
	Ours	10	84.84±0.33	89.53±0.13	89.44±0.01	91.35±0.12	92.01±0.28
	Ours	100	**87.24±0.51**	**90.86±0.05**	**91.29±0.26**	**92.11±0.15**	**92.65±0.10**

Table 4: Test accuracy for different evaluation methods on different datasets using foundation model CLIP (backbone ViT-L). We do not use data augmentation for LP. We evaluate FT without data augmentation, with 10 augmentation and with 100 augmentation to each training images. For Ours, we use 10, 100 augmentation.

C.4 Improving the Trade-off: Finetune with Contrastive Regularization

Evaluation & Methods. We use the feature extractor (ResNet18) pre-trained as in Section 3.1 by MoCo v2. Then, we report three evaluation methods, Linear Probing (LP), Finetune (FT), and Finetune with Contrastive Regularization (Ours) on CIFAR-10 under different percentages of labeled data as in Appendix C.2. LP follows the training protocol in Section 3.1. FT and Ours learn a linear predictor and update the representation, and use the same data augmentation for fair comparison. FT follows the training in MAE (He et al., 2022) mostly, using SGD for 200 epochs with a cosine learning-rate scheduler, base learning rate of 0.06, weight decay 5e-4, momentum 0.9 and batch size 256. Moreover, ours uses the contrastive loss from MoCo v2 and regularization coefficient $\lambda = 0.1$.

Results. In Table 3, the trade-off phenomenon also exists for FT evaluation, where the FT test accuracy drops when the pre-training dataset contains more diverse data points. Table 3 shows that Ours can achieve better performance than the other baselines. In particular, it outperforms the typical fine-tuning method consistently, even when the latter also uses the same amount data augmentation. This confirms the benefit by the contrastive regularization. Contrastive regularization can down-weight the downstream task-irrelevant invariant feature, so it can improve the model generalization ability, which is consistent with the discussion in Section 2.2.

C.4.1 Larger Foundation Models

We verify our method's effectiveness in real-world scenarios. When users use foundation models, they cannot access the model and can only call the official API, (e.g. GPT-3, DALL·E (Ramesh et al., 2022)). The pricing for GPT-3 to get feature embedding is \$0.20 / 1k tokens. If users would like to use a foundation model on their downstream task, the most efficient way is to get feature embedding of their data from the API and train a small model, called adapter (Hu et al., 2021; Sung et al., 2022), on these embedding rather than on raw input data.

We evaluate CLIP (with ViT-L as the representation backbone), MoCo v3 (ViT-B backbone), and SimCSE (Gao et al., 2021) (BERT backbone). They are trained on (image, text), (image, image), and (text, text) contrastive pairs, respectively, so cover a good spectrum of methods.

For CLIP and MoCo v3, we fix the backbone for all evaluation methods. For LP, we add a linear FC layer on top of the backbone. For FT and Ours, we insert a two-layer ReLU neural network (1024 dimension for hidden layer) as an adapter between the backbone and the linear classification

Target data	Method	Aug	1% label data	5% label data	10% label data	20% label data	100% label data
CIFAR-10	LP	1	**91.44±0.01**	93.51±0.01	94.11±0.01	94.22±0.01	95.82±0.01
	FT	1	89.93±0.38	94.21±0.35	95.15±0.06	95.80±0.06	96.12±0.11
	FT	10	90.82±0.19	93.24±0.08	94.59±0.08	95.48±0.01	96.17±0.12
	FT	100	90.84±0.03	93.05±0.02	94.23±0.08	95.37±0.01	**97.01±0.07**
	Ours	10	90.73±0.18	**94.28±0.03**	**95.43±0.15**	**95.83±0.14**	96.71±0.10
	Ours	100	91.04±0.06	94.00±0.06	95.29±0.01	95.72±0.05	96.86±0.06
SVHN	LP	1	39.40±0.02	50.50±0.02	54.61±0.02	57.66±0.01	61.92±0.01
	FT	1	38.82±0.10	48.15±0.37	51.03±0.14	52.07±0.09	56.19±0.33
	FT	10	45.00±0.34	52.61±0.24	54.45±0.12	57.05±0.11	65.36±0.33
	FT	100	45.70±0.13	54.51±0.23	57.76±0.01	61.13±0.39	69.10±0.39
	Ours	10	**46.53±0.23**	55.59±0.03	57.32±0.05	59.20±0.09	66.29±0.20
	Ours	100	46.27±0.09	**55.70±0.07**	**59.45±0.04**	**61.97±0.13**	**70.22±0.01**
GTSRB	LP	1	48.52±0.03	66.68±0.02	71.69±0.01	72.27±0.02	75.37±0.01
	FT	1	52.54±0.67	72.19±0.33	73.75±0.71	73.30±0.46	75.16±0.01
	FT	10	58.68±0.01	75.21±0.23	75.87±0.06	76.75±0.28	76.45±0.29
	FT	100	61.65±0.16	75.22±0.77	76.49±0.31	77.67±0.63	78.05±0.30
	Ours	10	59.28±0.04	75.35±0.31	77.38±0.09	**80.52±0.12**	**81.28±0.10**
	Ours	100	**63.61±0.92**	**76.70±0.17**	**77.85±0.23**	80.13±0.01	80.92±0.19

Table 5: Test accuracy for different evaluation methods on different datasets using foundation model MoCo v3 (backbone ViT-B). We do not use data augmentation for LP. We evaluate FT without data augmentation, with 10 augmentation and with 100 augmentation to each training images. For Ours, we use 10, 100 augmentation.

Target data	Method	1% label data	5% label data	10% label data	20% label data	100% label data
IMDB	LP	79.72±0.06	83.08±0.20	81.48±0.89	84.87±0.03	86.49±0.16
	FT	82.54±2.88	87.78±0.42	87.96±1.27	89.49±1.02	92.31±0.26
	Ours	**84.48±1.62**	**90.12±0.41**	**90.41±0.49**	**90.79±1.58**	**92.85±0.03**
AGNews	LP	85.52±0.31	86.78±0.62	86.75±0.66	87.62±0.24	87.76±0.66
	FT	88.74±0.34	90.76±0.70	91.22±0.07	92.36±0.14	93.57±0.23
	Ours	**89.20±0.72**	**91.22±0.06**	**91.33±1.33**	**92.45±0.01**	**93.94±0.02**

Table 6: Test accuracy for different evaluation methods on different datasets using foundation model SimCSE (backbone BERT). We do not use data augmentation for LP. We evaluate FT and Ours with the same data augmentation as SimCSE.

layer. For Ours, we apply SimCLR contrastive loss on the adapted feature (output of adapter) and set $\lambda = 1.0$. We use the same training strategy as Section 3.1 for LP and as Table 3 for FT and Ours. In line with the actual situation, we control the number of augmentation number used in FT and Ours (more data augmentation leading to higher price in practice).

We conduct experiments on NLP tasks as well. SimCSE proposes a contrastive learning method for sentence embeddings, which uses the dropout feature from BERT as data augmentation. The max sequence embedding length is 512. For SimCSE, all three evaluation methods use a linear classifier. For all evaluation methods, we use AdamW (Loshchilov & Hutter, 2018) with weight decay $= 0.01$ and train 3 epochs with batch size 16. For LP, we fix the backbone and set learning rate as 5e-3. For FT and Ours, we train the backbone and linear classification layer simultaneously using unique data augmentation in each training step and set learning rate as 5e-5. For Ours, we apply SimCSE contrastive loss on the feature (output of the backbone) and set $\lambda = 1.0$.

As in Appendix C.2, we report LP, FT and Ours on $1\%, 5\%, 10\%, 20\%, 100\%$ of the labeled data from the downstream task in Table 4, Table 5 and Table 6 for CLIP, MoCo v3 and SimCSE respectively. For CLIP and MoCo v3 in Table 4 and Table 5, we consider different data augmentation numbers, e.g. 10, 100. For SimCSE, we use the standard data augmentation, i.e. generating unique augmentation for each gradient step.

Three tables again show our method can consistently improve the downstream prediction performance in all three real-world scenarios, and quite significantly in some cases (e.g., MoCo v3 on GTSRB). This shows that the method is also useful for large foundation models, including the case when the foundation models cannot be fine-tuned and only the extracted embeddings can be adapted.

C.5 More Figure of Verifying the Existence of the Trade-off

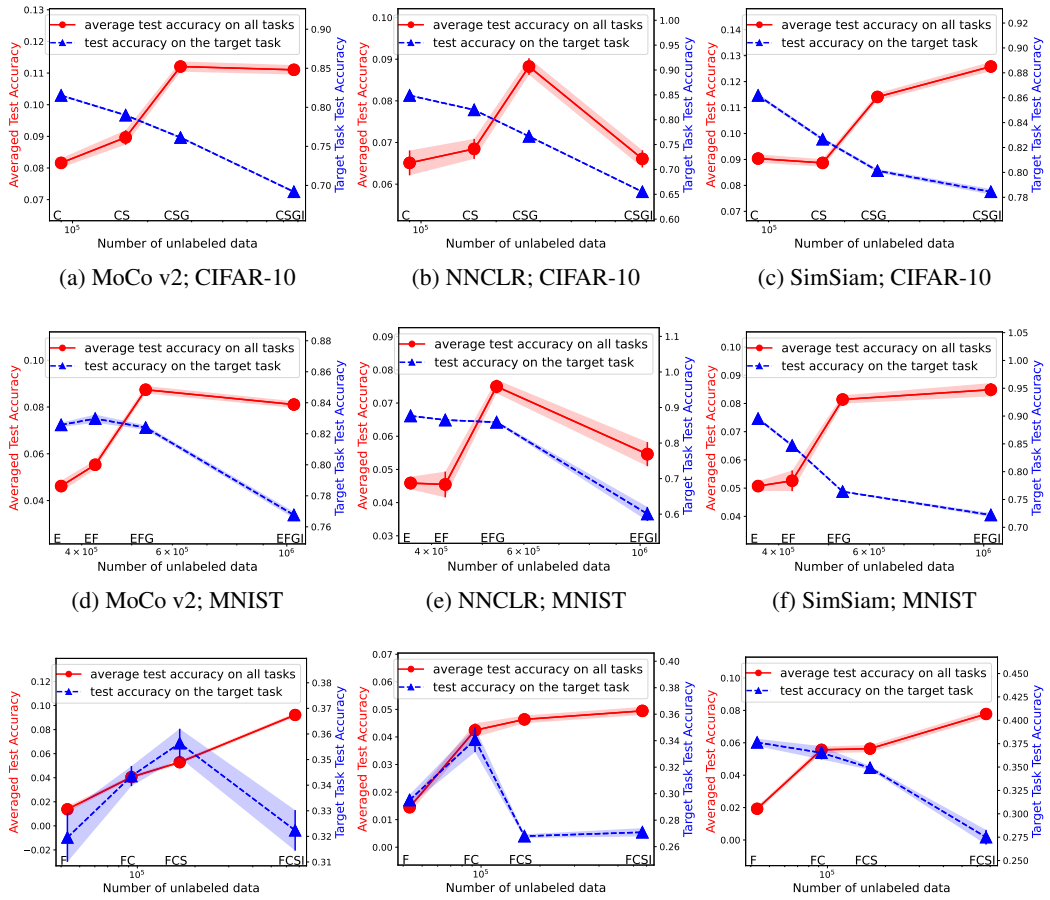

(a) MoCo v2; CIFAR-10 (b) NNCLR; CIFAR-10 (c) SimSiam; CIFAR-10

(d) MoCo v2; MNIST (e) NNCLR; MNIST (f) SimSiam; MNIST

(g) MoCo v2; Fer2013 (h) NNCLR; Fer2013 (i) SimSiam; Fer2013

Figure 12: Trade-off of universality and label efficiency for MoCo v2, NNCLR, SimSiam on downstream tasks CIFAR-10, MNIST, Fer2013. x-axis: incrementally add datasets for pre-training. Pre-training data: (a)(b)(c) CINIC-10 (C), SVHN (S), GTSRB (G), and ImageNet32 (I). For example, "CS" on the x-axis means CINIC-10+SVHN. Target task: CIFAR-10. Red line: average test accuracy of Linear Probing on all 4 datasets. Blue line: test accuracy on the target task. (d)(e)(f) EMNIST-Digits&Letters (E), Fashon-MNIST (F), GTSRB (G), ImageNet32 (I). Target: MNIST. (g)(h)(i) FaceScrub (F), CIFAR-10 (C), SVHN (S), ImageNet32 (I). Target: Fer2013. All evaluations are trained with 1% labeled data.

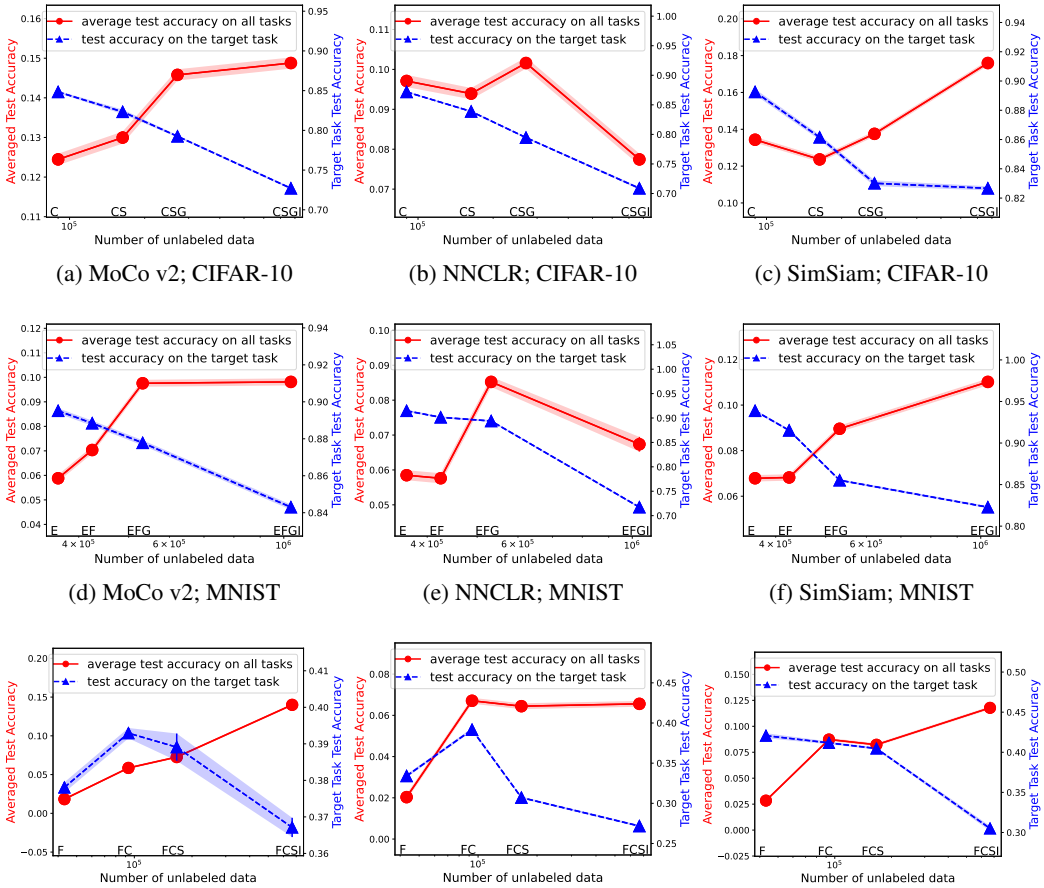

(a) MoCo v2; CIFAR-10 (b) NNCLR; CIFAR-10 (c) SimSiam; CIFAR-10

(d) MoCo v2; MNIST (e) NNCLR; MNIST (f) SimSiam; MNIST

(g) MoCo v2; Fer2013 (h) NNCLR; Fer2013 (i) SimSiam; Fer2013

Figure 13: Trade-off of universality and label efficiency for MoCo v2, NNCLR, SimSiam on downstream tasks CIFAR-10, MNIST, Fer2013. x-axis: incrementally add datasets for pre-training. Pre-training data: (a)(b)(c) CINIC-10 (C), SVHN (S), GTSRB (G), and ImageNet32 (I). For example, "CS" on the x-axis means CINIC-10+SVHN. Target task: CIFAR-10. Red line: average test accuracy of Linear Probing on all 4 datasets. Blue line: test accuracy on the target task. (d)(e)(f) EMNIST-Digits&Letters (E), Fashon-MNIST (F), GTSRB (G), ImageNet32 (I). Target: MNIST. (g)(h)(i) FaceScrub (F), CIFAR-10 (C), SVHN (S), ImageNet32 (I). Target: Fer2013. All evaluations are trained with 5% labeled data.

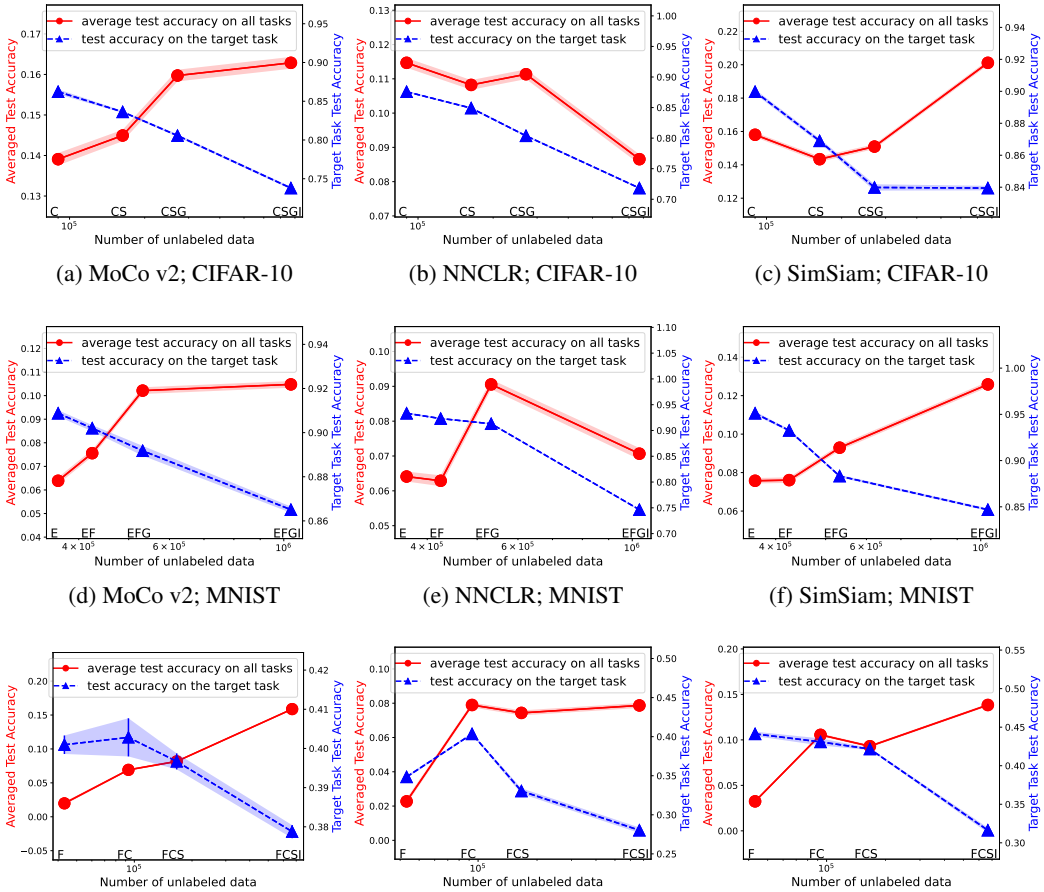

(a) MoCo v2; CIFAR-10 (b) NNCLR; CIFAR-10 (c) SimSiam; CIFAR-10

(d) MoCo v2; MNIST (e) NNCLR; MNIST (f) SimSiam; MNIST

(g) MoCo v2; Fer2013 (h) NNCLR; Fer2013 (i) SimSiam; Fer2013

Figure 14: Trade-off of universality and label efficiency for MoCo v2, NNCLR, SimSiam on downstream tasks CIFAR-10, MNIST, Fer2013. x-axis: incrementally add datasets for pre-training. Pre-training data: (a)(b)(c) CINIC-10 (C), SVHN (S), GTSRB (G), and ImageNet32 (I). For example, "CS" on the x-axis means CINIC-10+SVHN. Target task: CIFAR-10. Red line: average test accuracy of Linear Probing on all 4 datasets. Blue line: test accuracy on the target task. (d)(e)(f) EMNIST-Digits&Letters (E), Fashon-MNIST (F), GTSRB (G), ImageNet32 (I). Target: MNIST. (g)(h)(i) FaceScrub (F), CIFAR-10 (C), SVHN (S), ImageNet32 (I). Target: Fer2013. All evaluations are trained with 10% labeled data.

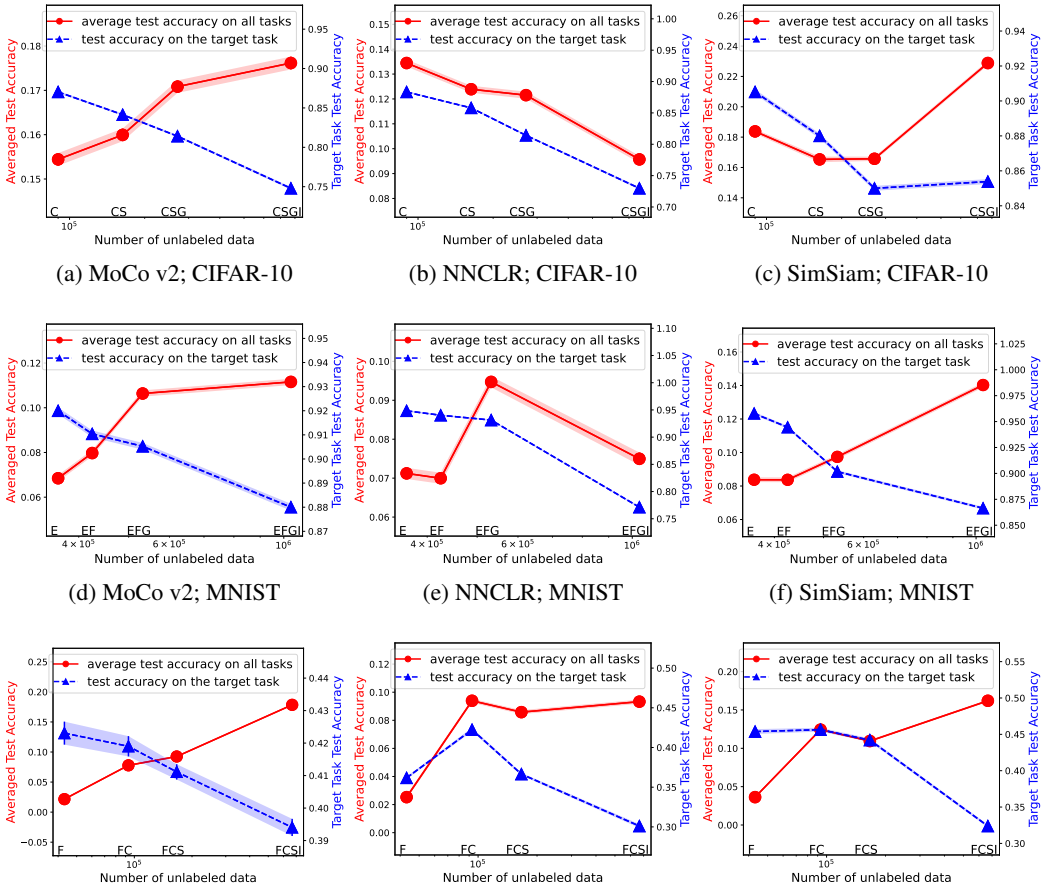

(a) MoCo v2; CIFAR-10 (b) NNCLR; CIFAR-10 (c) SimSiam; CIFAR-10

(d) MoCo v2; MNIST (e) NNCLR; MNIST (f) SimSiam; MNIST

(g) MoCo v2; Fer2013 (h) NNCLR; Fer2013 (i) SimSiam; Fer2013

Figure 15: Trade-off of universality and label efficiency for MoCo v2, NNCLR, SimSiam on downstream tasks CIFAR-10, MNIST, Fer2013. x-axis: incrementally add datasets for pre-training. Pre-training data: (a)(b)(c) CINIC-10 (C), SVHN (S), GTSRB (G), and ImageNet32 (I). For example, "CS" on the x-axis means CINIC-10+SVHN. Target task: CIFAR-10. Red line: average test accuracy of Linear Probing on all 4 datasets. Blue line: test accuracy on the target task. (d)(e)(f) EMNIST-Digits&Letters (E), Fashon-MNIST (F), GTSRB (G), ImageNet32 (I). Target: MNIST. (g)(h)(i) FaceScrub (F), CIFAR-10 (C), SVHN (S), ImageNet32 (I). Target: Fer2013. All evaluations are trained with 20% labeled data.

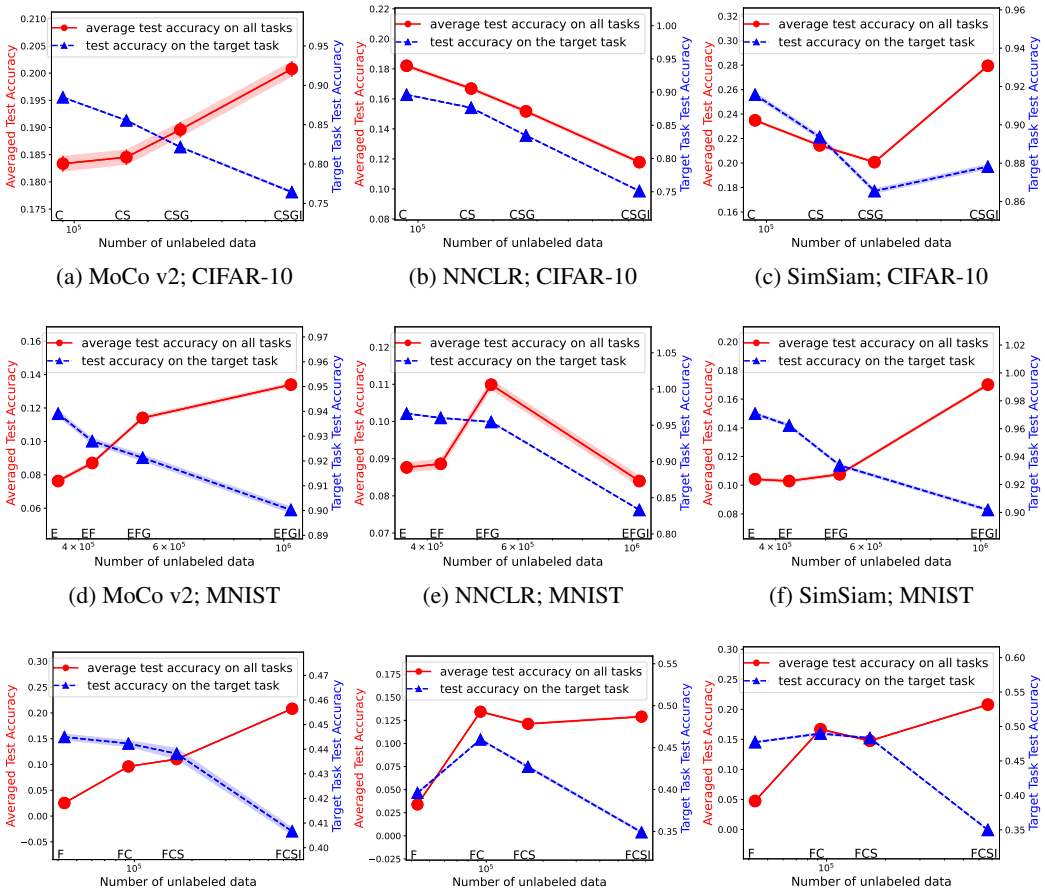

(a) MoCo v2; CIFAR-10 (b) NNCLR; CIFAR-10 (c) SimSiam; CIFAR-10

(d) MoCo v2; MNIST (e) NNCLR; MNIST (f) SimSiam; MNIST

(g) MoCo v2; Fer2013 (h) NNCLR; Fer2013 (i) SimSiam; Fer2013

Figure 16: Trade-off of universality and label efficiency for MoCo v2, NNCLR, SimSiam on downstream tasks CIFAR-10, MNIST, Fer2013. x-axis: incrementally add datasets for pre-training. Pre-training data: (a)(b)(c) CINIC-10 (C), SVHN (S), GTSRB (G), and ImageNet32 (I). For example, "CS" on the x-axis means CINIC-10+SVHN. Target task: CIFAR-10. Red line: average test accuracy of Linear Probing on all 4 datasets. Blue line: test accuracy on the target task. (d)(e)(f) EMNIST-Digits&Letters (E), Fashon-MNIST (F), GTSRB (G), ImageNet32 (I). Target: MNIST. (g)(h)(i) FaceScrub (F), CIFAR-10 (C), SVHN (S), ImageNet32 (I). Target: Fer2013. All evaluations are trained with 100% labeled data.